Human Molecular Genetics, 2017, Vol. 26, No. 7 1230–1246

doi: 10.1093/hmg/ddx028
Advance Access Publication Date: 1 February 2017
Original Article

ORIGINAL ARTICLE

Therapeutic potential of AAV-mediated MMP-3 secretion from corneal endothelium in treating glaucoma

Jeffrey O'Callaghan[1,*], Darragh. E. Crosbie[1], Paul. S. Cassidy[1], Joseph M. Sherwood[2], Cassandra Flügel-Koch[3], Elke Lütjen-Drecoll[3], Marian M. Humphries[1], Ester Reina-Torres[1], Deborah Wallace[4], Anna-Sophia Kiang[1], Matthew Campbell[1], W. Daniel Stamer[5], Darryl R. Overby[2], Colm O'Brien[6], Lawrence C. S. Tam[1,*,†] and Peter Humphries[1,*,†]

[1]Ocular Genetics Unit, Smurfit Institute of Genetics, University of Dublin, Trinity College, Dublin, D2, Ireland, [2]Department of Bioengineering, Imperial College London, London, SW7 2BX, UK, [3]Department of Anatomy II, University of Erlangen-Nürnberg, D-91054 Erlangen, Germany, [4]Clinical Research Centre, UCD School of Medicine and Medical Science, University College Dublin, Belfield, Dublin 4, Ireland, [5]Departments of Ophthalmology and Biomedical Engineering, Duke University, Durham, NC, USA and [6]Department of Ophthalmology, Mater Misericordiae University Hospital, Dublin, D7, Ireland

*To whom correspondence should be addressed: Tel: 353 1 896 2164, 353 1 896 1547; Fax: 353 1 679 8558; E-mail: ocallaje@tcd.ie (J.O.), lawrenct@tcd.ie (L.C.S.T.), pete.humphries@tcd.ie (P.H.)

Abstract

Intraocular pressure (IOP) is maintained as a result of the balance between production of aqueous humour (AH) by the ciliary processes and hydrodynamic resistance to its outflow through the conventional outflow pathway comprising the trabecular meshwork (TM) and Schlemm's canal (SC). Elevated IOP, which can be caused by increased resistance to AH outflow, is a major risk factor for open-angle glaucoma. Matrix metalloproteinases (MMPs) contribute to conventional aqueous outflow homeostasis in their capacity to remodel extracellular matrices, which has a direct impact on aqueous outflow resistance and IOP. We observed decreased MMP-3 activity in human glaucomatous AH compared to age-matched normotensive control AH. Treatment with glaucomatous AH resulted in significantly increased transendothelial resistance of SC endothelial and TM cell monolayers and reduced monolayer permeability when compared to control AH, or supplemented treatment with exogenous MMP-3.

Intracameral inoculation of AAV-2/9 containing a CMV-driven MMP-3 gene (AAV-MMP-3) into wild type mice resulted in efficient transduction of corneal endothelium and an increase in aqueous concentration and activity of MMP-3. Most importantly, AAV-mediated expression of MMP-3 increased outflow facility and decreased IOP, and controlled expression using an inducible promoter activated by topical administration of doxycycline achieved the same effect. Ultrastructural analysis of MMP-3 treated matrices by transmission electron microscopy revealed remodelling and degradation of core extracellular

†These authors contributed equally to this work.

Received: December 9, 2016. **Revised:** January 17, 2017. **Accepted:** January 18, 2017

matrix components. These results indicate that periodic induction, via use of an eye drop, of AAV-mediated secretion of MMP-3 into AH could have therapeutic potential for those cases of glaucoma that are sub-optimally responsive to conventional pressure-reducing medications.

Introduction

The eye is pressurised by a balance in the production of aqueous humour (AH) by the ciliary processes and resistance to its drainage through the trabecular meshwork (TM) and Schlemm's canal (SC). Located at the apex of the iridocorneal angle, SC is a flattened circular vessel with an average meridional diameter of 233 μm in humans (1). AH exits the lumen of SC into collector channels and drains into the episcleral veins that are visible on the surface of the sclera. Precise regulation of aqueous inflow together with outflow resistance is critical in maintaining an average intraocular pressure (IOP) of approximately 16 mmHg in a normal functioning eye (2). In cases of primary open-angle glaucoma (POAG), so-called because the iridocorneal angle remains open without noticeable physical obstruction, resistance to AH drainage through the TM and SC is increased by mechanisms that have yet to be fully elucidated, resulting in elevated IOP (3). This, in turn, results in deformation of the lamina cribrosa—the tissue that structurally supports the optic nerve head—(often referred to as 'cupping' of the optic nerve head), damaging retinal ganglion cell axons, leading to ganglion cell degeneration and irreversible blindness.

Lowering IOP remains the only effective treatment for POAG. Topical pressure reducing medications either increase the rate of aqueous outflow through the conventional or unconventional pathway, or reduce aqueous production (3). The U.S. spends $1.9 billion per annum to treat glaucoma, 38–52% of such costs being related to topical pressure reducing medications (4). However, such medications often do not reduce IOP to the desired target pressure and may induce side effects in certain patients. Such patients may then undergo surgical interventions, which have associated risks and complications. Hence, there remains an unmet clinical need for improved methods of disease treatment.

Functional studies have provided evidence that the generation of aqueous outflow resistance is most significant in the juxtacanalicular tissue (JCT—the outer layer of the TM) and inner wall endothelium of SC (5,6). In particular, the extracellular matrix (ECM) composition in the JCT region has been shown to influence outflow patterns and resistance generation (6–11). Competitive disruption or inhibition of integrin-ECM linkages that attach the cell to the ECM, or inhibition of ECM receptors have been associated with increases in endothelial monolayer permeability and transendothelial transport (12–15). This implicates features that are relevant to SC endothelial cells (SCEC) and their supporting basement membrane, such as integrin-ECM interactions, along with other inter-endothelial junctions that govern cell shape, in the control of endothelial paracellular permeability (16). TM cells play an integral role in modulating the ECM of the JCT to preserve AH flow pathways via continual and signal-initiated ECM remodelling (17). The ECM in the JCT region is comprised of a heterogeneous group of fibrous and matrical materials including collagen type IV, proteoglycans, laminin and fibronectin, all of which provide tensile strength and support to surrounding cells. The cribriform plexus, a structure composed of elastic fibres, connects the inner wall endothelium and the ciliary muscle, allowing for JCT expansion in response to IOP elevation (18). ECM reconditioning of these matrix networks can thus induce changes in the actin cytoskeleton through integrin-ECM linkages, enabling F-actin or alpha-smooth muscle actin (α-SMA) to act as markers for active ECM remodelling (19–21). ECM turnover in the conventional outflow pathway is regulated by a family of zinc-dependent endopeptidases, the matrix metalloproteinases (MMPs). These secreted proteases are responsible for the degradation of ECM proteins and cell proliferation, and are thus key components in ECM remodelling and outflow tissue homeostasis (22). MMPs are secreted as inactive protein precursors and are activated when cleaved by extracellular proteinases and other MMPs (23). Levels of MMPs, along with TIMPs (Tissue Inhibitors of Metalloproteinases), have been shown to differ in glaucomatous AH and TM tissue as compared to those from normotensive individuals (24,25). Imbalance in MMP/TIMP ratios, and reduced MMP enzymatic activity, has been correlated with the accumulation of ECM materials in the TM that ultimately leads to an increase in outflow resistance (26,27). Therefore, reduction in ECM turnover within the TM and JCT region as a result of an imbalanced latent-to-activated MMP ratio can be a contributing factor to increased outflow resistance, as observed in glaucoma. It is therefore evident that increasing ECM turnover in outflow tissues may have therapeutic significance by reducing outflow resistance. Here, we set out to develop a gene-based therapy for the delivery of MMP targeting the conventional outflow tissues, with the primary aim of reducing both outflow resistance and IOP. Introduction of MMPs into the anterior chamber of the eye has previously been shown to increase outflow facility in organ-perfused cultures, indicating their therapeutic potential (28–31). Of the many classes of MMPs, MMP-3 (stromelysin-1) presents itself as an attractive candidate for targeting the ECM of outflow tissues. MMP-3 possesses a vast proteolytic target profile including type IV collagen, fibronectin, laminin, elastin, and proteoglycans, all of which are present in the meshwork and JCT regions of the outflow tissues, making this MMP of particular interest (32–36). In addition, MMP-3 can also activate other MMPs, including MMP-1 and MMP-9 (23,37–39), further assisting in the remodelling of ECM components (40–42).

Efficient gene delivery into the anterior segment of the eye is feasible through the use of adenoviral and adeno-associated viral (AAV) vectors. In particular, self-complementary AAV vectors have been shown to have such capability (43–46). Owing to the fact that MMP-3 is a secretory enzyme synthesised in the endoplasmic reticulum, transduction of tissues of the anterior segment with AAV expressing MMP-3 will result in the secretion of the protein into the AH. This will subsequently enable MMP-3 to be delivered into outflow tissues via conventional aqueous flow, potentially facilitating targeted degradation of ECM components and thus increasing aqueous outflow. In this regard, we observed highly efficient transduction of corneal endothelial cells following a single intracameral inoculation of AAV-2/9 expressing MMP-3, and both levels and activity of MMP-3 were significantly elevated in mouse AH following such inoculation. Importantly, AAV-mediated expression of MMP-3 in corneal endothelium, either from a CMV-, or doxycycline-inducible promoter, resulted in a marked increase in outflow facility and reduction in IOP. These observations correlated with structural alterations in the ECM of the outflow tissues, suggesting a mechanism of action for MMP-3 in modulating outflow resistance.

Results

Effects of glaucomatous aqueous humour on SC endothelial and TM cell monolayers

We treated cultured human SCEC monolayers with human glaucomatous (POAG) or control (cataract) AH for 24 h, and quantified levels of total secreted and activated MMP-3 in culture media. This was achieved by performing an ELISA and FRET assay, to monitor the degree of cleavage of an MMP-3 specific substrate, on cell media 24 h post-treatment. We did not observe a significant increase in the level of total (latent and active forms) secreted MMP-3 in culture media following treatment with POAG aqueous, with an increase of 0.15 [−0.35, 0.66] ng/ml (mean [95% confidence interval (CI)]) ($P = 0.45$, $n = 3$, Fig. 1A) over controls. However, activity assays indicated that the MMP-3 secreted in response to POAG aqueous had less enzymatic activity than that of cataract control AH, with an average change of −0.15 [−0.28, −0.02] mU/ml ($P = 0.024$, $n = 9$ cataract, $n = 7$ POAG, Fig. 1B). These observations corroborate results obtained involving other members of the MMP family in POAG aqueous (24) in that the amount of secreted MMP may remain relatively unchanged but its proteolytic activity is reduced.

Effects of glaucomatous AH on the permeability of SCEC and human TM (HTM) monolayers were determined by trans-endothelial electrical resistance (TEER) and FITC-dextran flux assays. Treatment of cultured SCEC monolayers with POAG AH resulted in increased TEER by an average of 102% after 24-h treatment compared to control AH (−7%), displaying an average absolute increase of 19.82 [15.82, 23.81] $\Omega.cm^2$ ($P < 0.0001$, $n = 6$ cataract, $n = 12$ POAG, Fig. 1C). Similarly, HTM responded with an increase of 9.79 [5.55, 14.05] $\Omega.cm^2$ in response to glaucomatous AH, ($P = 0.0002$, $n = 8$, Fig. 1D). Glaucomatous AH also reduced paracellular flux, as measured by permeability co-efficient (P_{app}), to dextran of 70 kDa as compared to cataract controls, with a mean difference of 0.14 [0.05, 0.22] cm/s $\times 10^{-8}$ ($P = 0.009$, $n = 3$ cataract, $n = 3$ POAG, Fig. 1E). A reduction in HTM permeability was also observed with a mean difference of 0.17 [0.09, 0.23] cm/s $\times 10^{-9}$ ($P = 0.005$, $n = 8$ cataract, $n = 7$ POAG, Fig. 1F).

Treatment of outflow cell monolayers with recombinant human MMP-3 increases permeability with concomitant reductions in TEER

In contrast to the negative effects of glaucomatous AH on SCEC and HTM permeability and resistance, we observed that treatment of cultured monolayers with 10 ng/ml of active recombinant human MMP-3 reduced TEER values on average by 5.62 [2.92, 8.32] $\Omega.cm^2$ greater than inactivated MMP-3 controls over the course of 24 h for SCEC ($P < 0.0001$, $n = 8$, Fig. 2A) and by 4.29 [0.11, 8.48] $\Omega.cm^2$ for HTM ($P = 0.0137$, $n = 8$, Fig. 2B) respectively. Permeability assays complemented these data as increases in paracellular flux of 70 kDa FITC-dextran by 0.14 [0.12, 0.18] cm/s $\times 10^{-9}$ ($P < 0.0001$, $n = 8$, Fig. 2C) were observed in SCEC, and 0.04 [0.01, 0.06] cm/s $\times 10^{-9}$ ($P < 0.01$, $n = 8$, Fig. 2D) in HTM monolayers when comparing treatments of MMP-3 to its inactivated counterpart control: TIMP-1 incubated with MMP-3. To rule out cytotoxicity as a reason for the observed changes in paracellular permeability, a cell viability assay was undertaken. Based on data shown in Figure 2E, for concentrations below 36 ng/ml MMP-3, the average SCEC cell viability for $n = 3$ will exceed 85%. Greater tolerability was observed in HTM cases, retaining an average viability of at least 85% for MMP-3 concentrations up to 151 ng/ml ($n = 3$, Fig. 2F).

Treatment of SCEC and HTM monolayers with active recombinant human MMP-3 induces remodelling and degradation of ECM components

In order to attribute increases in permeability to the ECM remodelling effects associated with MMP-3, SCEC and HTM monolayers were both treated as above with 10 mg/ml MMP-3 for 24 h. Following treatment, we observed changes in the staining pattern and intensity of a number of ECM proteins by immunocytochemistry. Specific collagen IV staining was localised to perinuclear areas and cytoplasm in both SCEC and HTM cells (Fig. 3A and B). In particular, we observed a decrease in the staining intensity around perinuclear areas in treated cells as compared to controls. A-SMA fibres facilitating cell-cell contacts in SCEC localised specifically to the cytoplasm and cytoskeleton, and MMP-3 treatment led to an attenuation of fibre bundles with thinning of intercellular connections (Fig. 3C). Fluorescent images of F-actin in HTM monolayers also revealed constricted actin bundles and a reduced tendency for bundle crossovers (Fig. 3D). Immunofluorescence staining of laminin in SCEC and HTM cells showed diminished cytoplasmic localisation and reduced network complexity and multiplicity in MMP-3 treated cells as compared to control staining intensity of laminin (Fig. 3E and F). To visualise fibronectin clearly without cellular interference, decellularisation was performed after MMP-3 treatment to isolate the ECM scaffold from the cell monolayer. Fluorescent images show significant perturbation of fibronectin network in treated cells as opposed to the linear cellular organisation observed in control cells (asterisk, Fig. 3G and H). To quantitatively demonstrate remodelling of these proteins, western blot analysis was performed on both cell lysate and media fractions of SC and HTM cell monolayers (Supplementary Material, Fig. S1). Specific bands were observed at 300 kDa for collagen IV, 42 kDa for α-SMA, 220 kDa for laminin and 290 kDa for fibronectin. A significant reduction of collagen IV ($P = 0.01$, $P = 0.01$) α-SMA ($P = 0.04$, $P = 0.04$) and laminin ($P = 0.04$, $P = 0.03$) were observed in SC and HTM whole cell lysate samples respectively ($n = 4$ for all cases). Collectively, these data clearly illustrate that MMP-3 mediates remodelling of ECM components in both SCEC and HTM cell monolayers.

Intracameral inoculation of AAV-2/9 expressing a CMV-driven MMP-3 gene efficiently transduces corneal endothelium and results in elevated levels of MMP-3 in aqueous humour

AAV-mediated transduction of corneal endothelium could, in principle, serve as an efficient means of expressing and secreting MMP-3 into AH. The advantage of such an approach is that the natural flow dynamics of AH will allow transportation of secreted MMP-3 towards the outflow tissues (Fig. 4A). We evaluated the efficiency of a number of AAV serotypes with either single stranded or self-complementary genomes to deliver MMP-3 to the outflow tissues. 2μl of viral particles (2×10^{12} vector genomes/ml) of each serotype, expressing a CMV-driven eGFP reporter gene (Fig. 4B) were intracamerally inoculated into wild type C57BL/6 mice and eyes examined via fluorescent microscopy at 3 weeks post-inoculation. Extensive expression of the reporter gene was observed in the corneal endothelium of eyes injected with non-self-complementary AAV-2/9 (Fig. 4C top), with no fluorescence being detectable in the outflow tissues themselves using this construct. Hence, the eGFP cDNA from AAV-2/9 was exchanged with murine MMP-3 cDNA to generate AAV-MMP-3, and similar inoculation resulted in MMP-3 expression that was prominently detected in the corneal

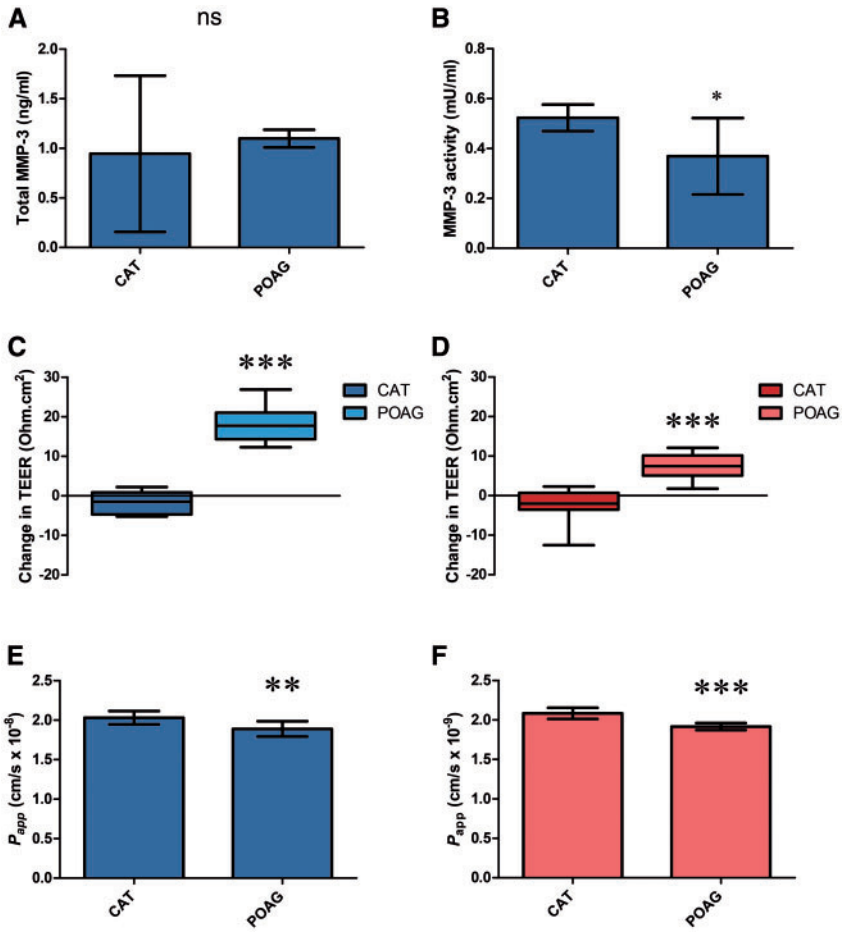

Figure 1. MMP-3 concentration in glaucomatous AH and the resulting effect on SCEC and HTM monolayers. (**A**) MMP-3 concentrations in the media of SCEC monolayers treated with either cataract (control) or POAG human AH showed no significant difference after 24 h. (**B**) POAG aqueous-treated SC media samples from (A) were found to have an average change in MMP-3 proteolytic activity of -0.15 [−0.28, −0.02] mU/ml compared to control media. (**C**) Addition of POAG aqueous humour onto SC monolayers resulted in an average increase in TEER of 102% compared to controls. (**D**) Treatment of HTM cells with human aqueous also increased TEER value. (**E,F**) SCEC and HTM subjected to AH were tested for cellular permeability using a FITC-Dextran flux assay respectively. Decreased permeability to a 70 kDa dextran was observed in response to POAG rather than cataract AH. Graphs show mean with 95% CI error bars. CAT = cataract, POAG = primary open-angle glaucoma. Figures A-F were analysed with a Student's *t*-test. NS = non-significant. Symbols *, ** and *** denote *P* values of < 0.05, < 0.01 and < 0.001, respectively.

endothelium and not in null controls (Fig. 4C, bottom). No significant difference in central corneal thickness was detected following AAV inoculation between treated (116.7 [112.5, 120.9] μm) and control eyes (116.4 [113.6, 119.1] μm) ($n = 4$, Supplementary Material, Fig. S2). Corneas also appeared clear with no signs of cataracts upon visual inspection.

The level of total MMP-3 in the AH of twelve inoculated animals was quantified using enzyme-linked immunosorbent assay (ELISA), and we observed a significant average increase in total MMP-3 protein of 56%, 1.37 [0.89, 1.84] ng/ml as compared to 0.87 [0.59, 1.12] ng/ml for control AAV ($P = 0.016$, $n = 12$, Fig. 4D). The activity of AAV-mediated production of MMP-3 was also assessed using FRET, and a significant increase in activity of 34 [6.86, 61.14] % was observed, on average, in AAV-MMP-3 treated eyes compared to contralateral controls ($P = 0.0164$, $n = 17$, Fig. 4E).

Intracameral inoculation of AAV-2/9 expressing an MMP-3 gene increases outflow facility and reduces IOP in murine eyes

In order to determine the effect of AAV-mediated expression of MMP-3 from the corneal endothelium on aqueous outflow, the conventional outflow facility was measured using the recently developed *iPerfusion* system designed specifically to measure conventional outflow facility in mice (47). Wild type mice were intracamerally injected with $1x10^{11}$ vector genomes of AAV-MMP-3, and contralateral eyes received the same quantity of AAV-Null. Four weeks post-inoculation, eyes were enucleated and perfused in pairs over incrementing steps in applied pressure. A representative flow-pressure plot provided in Supplementary Material, Figure S3A describes the relationship between flow rate (Q) at each pressure (P) step in both AAV-MMP-3 (red) and AAV-Null (blue) eyes. Furthermore, the relative percentage difference in facility within each data pair is depicted in Supplementary Material, Figure S3B (left). The resulting facility data presented in Figure 5A and B clearly illustrate that control eyes have an average facility of 8.44 [6.14, 11.60] nl/min/mmHg with treated eyes having an average facility of 11.73 [8.05, 17.08] nl/min/mmHg. There is, therefore, an average increase in outflow facility of 39 [19, 63] % in pairs, between treated eyes and their contralateral controls ($P = 0.002$, $n = 8$ pairs).

As the major pathology in POAG is IOP elevation, and an increased outflow facility was observed, tonometric IOP

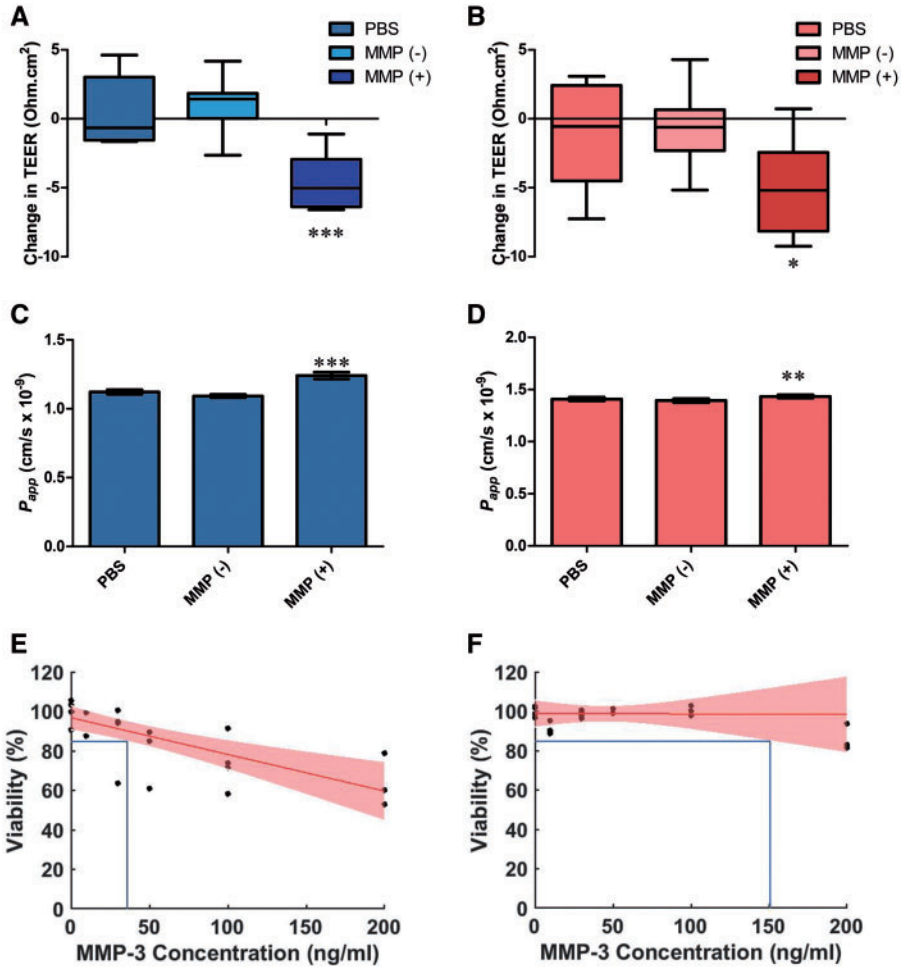

Figure 2. Effect of recombinant human MMP-3 on paracellular permeability in HTM and SCEC cell monolayers. SCEC and HTM cells were treated with 10 ng/ml recombinant MMP-3 for 24 h, using PBS and inactivated MMP-3 (incubation with TIMP-1, MMP(−)) as vehicle and negative controls respectively. (**A**) SCEC and (**B**) HTM both show reductions in TEER values after treatment of 4.6 [2.9, 6.2] and 5 [2.2, 7.8] Ohms.cm^2 respectively. Permeability to a 70 kDa dextran was increased in treated cells (MMP (+)) in both (**C**) SCEC and (**D**) HTM. (**E**) An average viability of 85% was expected for SCEC with MMP-3 concentrations up to 36 ng/ml. (**F**) 85% viability is retained on average in HTM cells at concentrations up to 151 ng/ml MMP-3. A, C and E in blue represent SCEC data, whereas B, D and F in red represent HTM data.

measurements were taken both immediately before (pre), and four weeks after (post) intracameral injection of AAV-2/9 expressing MMP-3 or a null vector in the case of the control. Differences between pre- and post-injection IOP were calculated using the non-parametric Wilcoxon matched-pairs signed rank test. Eyes treated with AAV-Null had no significant change in IOP -0.5 ± 2.9 mmHg (median ± median absolute deviation (MAD), $P = 0.61$, $n = 7$, Wilcoxon signed-rank test with a theoretical median IOP change of 0) after treatment. In comparison, when treated with AAV-MMP-3, median IOP significantly decreased by 3.0 ± 2.9 mmHg ($P = 0.022$, $n = 7$, Fig. 5C). The IOP difference in AAV-MMP-3 treated eyes was significantly greater than the IOP difference in the contralateral AAV-Null treated eyes by 2.5 ± 0.7 mmHg ($P = 0.034$, $n = 7$, Fig. 5C).

Controlled periodic activation of MMP-3

To incorporate a control mechanism for the secretion of MMP-3 from corneal endothelium, we first introduced AAV-2/9 expressing eGFP under the control of a tetracycline-inducible promoter into the anterior chambers of both eyes of wild type mice. After 3 weeks, mice were treated with a regime of one drop of 0.2% doxycycline (a tetracycline derivative) two times per day (approx. 8 h between each application) for 10–16 days in one eye only. PBS was administered onto the contralateral eye as a control. As illustrated in Supplementary Material, Figure S4, extensive expression of the reporter gene was observed only in the corneal endothelium, and no expression was observed in the contralateral control. Following this, we replaced the reporter cDNA with murine MMP-3 cDNA and the resulting AAV (Induc. AAV-MMP-3) was injected into the anterior chambers of animals at 1x10^{11} viral genomes per eye. Using the inducible eGFP virus (Induc. AAV-eGFP) as a contralateral control, expression was induced by administering doxycycline (as above) to both eyes. Contralateral eyes were perfused as above, the control group exhibiting an average facility of 8.30 [5.75, 11.26] nl/min/mmHg and the MMP-3 treatment group resulting in a facility of 14.01 [11.09, 17.72] nl/min/mmHg. Paired, these eyes exhibit an average increase in outflow facility of 68 [24, 128] % ($P = 0.004$, $n = 11$, Fig. 5D and E). The relative difference in facility within individual pairs is presented in Supplementary Material, Figure S3B (right). This observation strongly supports the concept that MMP-3 expression could be induced in a controlled and reversible manner, with periodic IOP measurements utilised to guide the induction of expression.

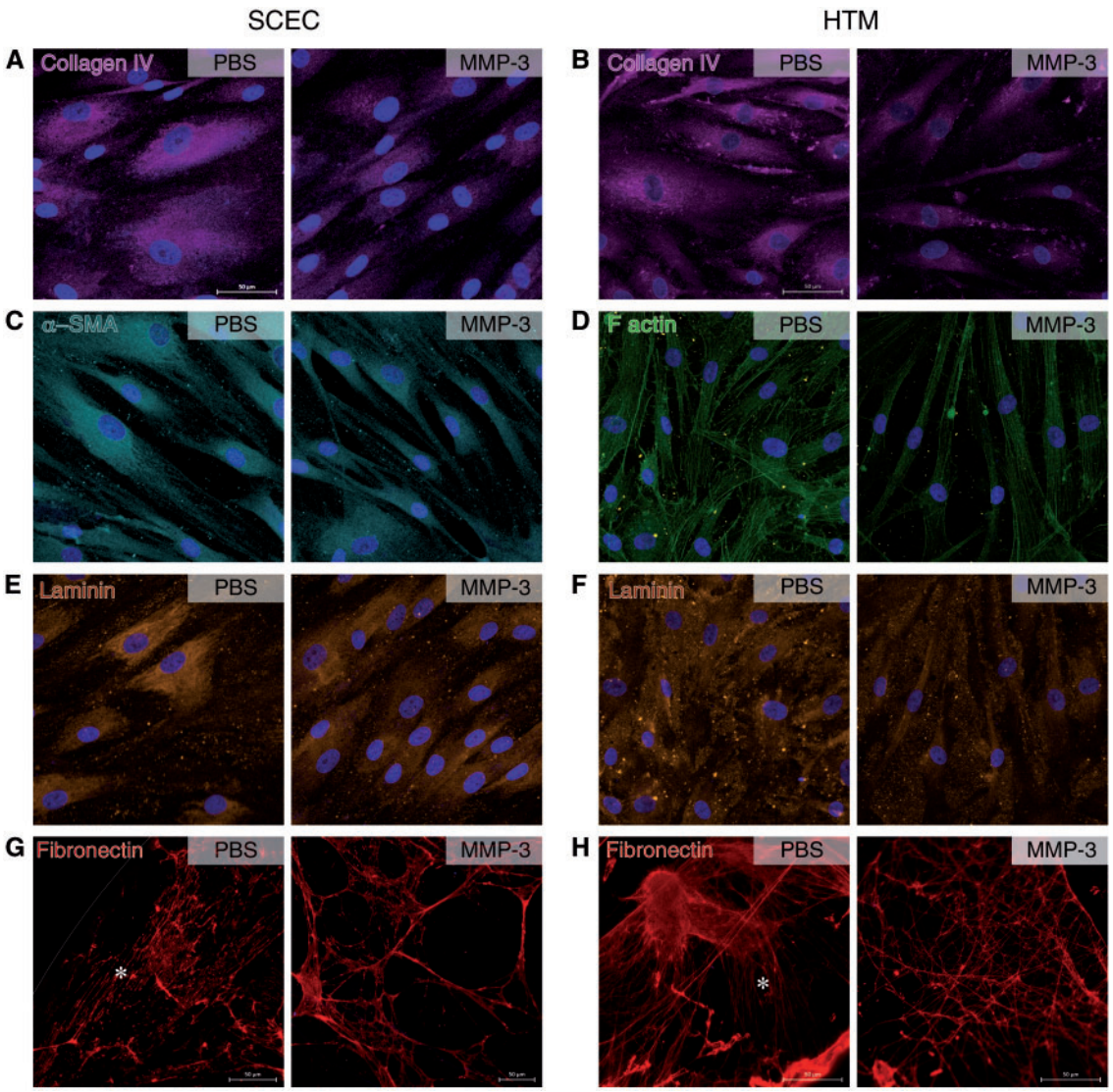

Figure 3. Remodelling of ECM components in SCEC and HTM cell monolayers. Immunocytochemistry shows various remodelling artefacts on core ECM components in SCEC and HTM cells in response to MMP-3 treatment. (**A,B**) Collagen IV appears to have reduced intensity in both cell types after treatment. Collagen IV is concentrated around cells in controls but shows reduced spread after treatment, fibrils barely protruding past the cell nuclei. (**C**) Alpha smooth muscle fibres extend the width of the cell towards a neighbouring cell. Treated samples show that these fibre bundles have constricted, leading to multiple thin connections between cells. (**D**) HTM F-actin staining depicts a slight thinning of filament bundles and a reduction of filament branching post MMP-3 treatment. (**E,F**) Laminin expression exhibits a modest reduction in staining intensity in both cell types, and a reduction in network complexity in TM cells. (**G,H**) Fibronectin was visualised after decellularisation, depicting linear and organised strands in PBS controls, as denoted by an asterisk. Treatment groups lacked a linear network, and instead showed a disjointed, porous network. Scale bars represent 50 μm. Left column pairs = SCEC, right column pairs = HTM.

Ultrastructural analysis of AAV-MMP-3 treated eyes

In order to evaluate whether the AAV-MMP-3 treatment affects the morphology of the eye and the TM including the inner wall of SC, ultrastructural investigation was performed in four pairs of mouse eyes. Corneas appeared translucent and healthy on visual inspection during enucleation. Semi-thin sections clearly demonstrated that there were no signs of an inflammatory reaction, either in the TM or in the cornea, uvea or retina (Fig. 6A and B). Ultrastructural analysis of control eyes revealed normal outflow structural morphology, cell-matrix attachments and cell-cell connections between the SC and TM. The inner wall endothelial cells formed foot-like connections with subendothelial TM cells, as well as connections to underlying elastic fibres and discontinuous basement membrane (Fig. 6C). However, in some regions of treated eyes, especially those with a prominent SC lumen and scleral spur-like structure typical of the nasal quadrant (48), there appeared to be more optically empty space directly underlying the inner wall endothelium of SC, compared to AAV-Null controls (Fig. 6D). In these optically empty spaces, foot-like extensions of the inner wall to the sub-endothelial layer were absent or disconnected from the subendothelial cells or elastic fibres (Fig. 6D and E). Occasionally, we observed an accumulation of ECM clumps beneath the inner wall that were not observed within the controls (Fig. 6F) and may represent remnants of digested material.

We quantified the optically empty length directly underlying the inner wall of SC. In control eyes, the percent optically empty length in any one region ranged from 19 to 49% with an average of 37%. In the treated eyes, the equivalent range was

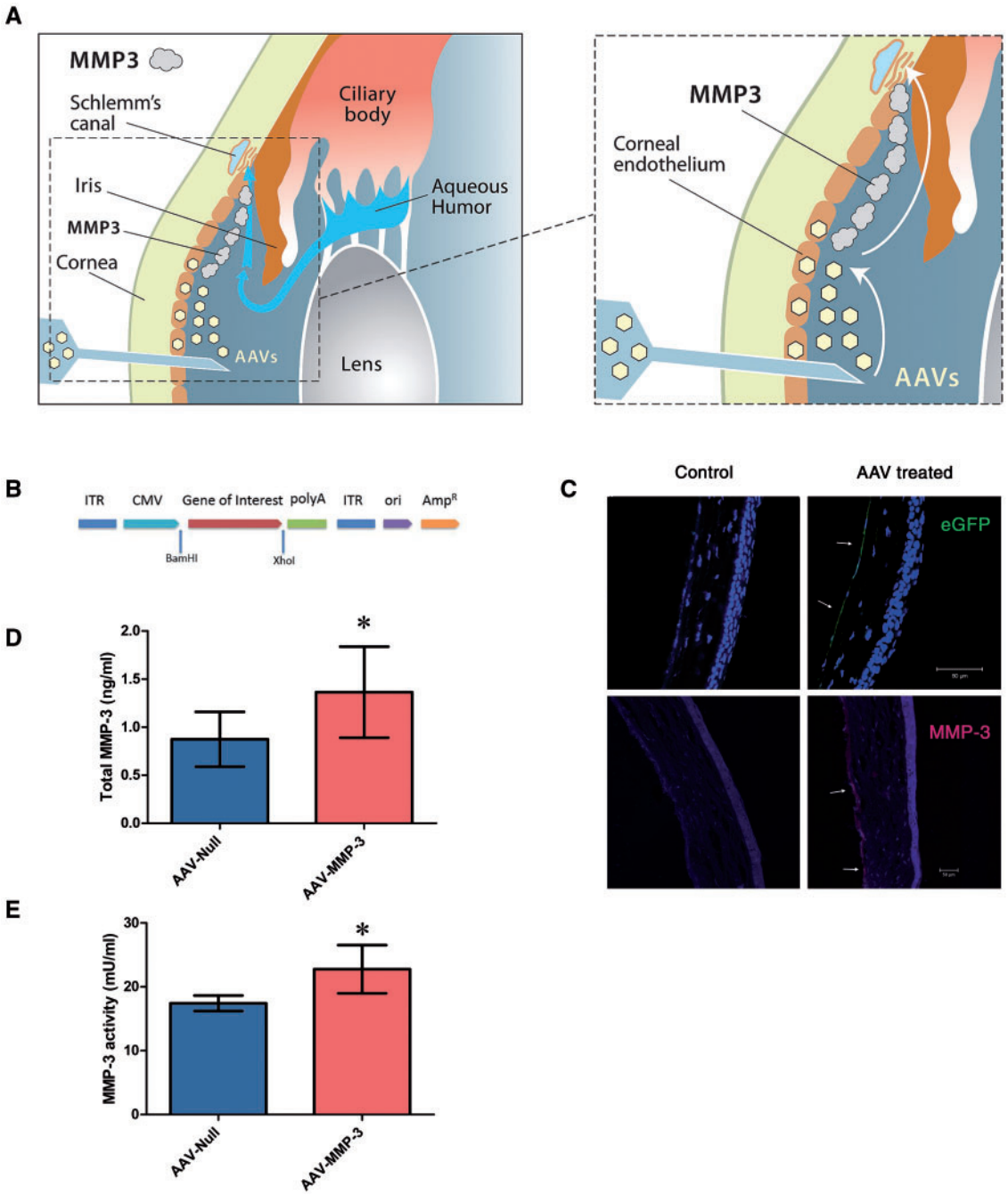

Figure 4. AAV-2/9 mediated MMP-3 expression in the corneal endothelium. (**A**) Diagrams illustrating the therapeutic concept addressed in this study. AAV-2/9 transduces the corneal endothelium upon intracameral inoculation (left). MMP-3 molecules are secreted into the AH from this location and are transported toward the outflow tissue by the natural flow of the aqueous (right). (**B**) A schematic diagram of the AAV-2/9 vector used for the expression of either eGFP or MMP-3. Murine MMP-3 cDNA was sub-cloned into the pAAV-MCS plasmid and constitutively driven by a CMV promoter (AAV-MMP-3). (**C**) Immunohistochemistry images of corneas from WT murine eyes intracamerally inoculated with AAV-2/9 expressing eGFP. AAV virus containing a CMV promoter demonstrates transduction and expression at the corneal endothelium (marked with arrows). Using the AAV-MMP-3 virus, MMP-3 was detected at the corneal endothelium in treated eyes only, denoted by arrows. (**D**) ELISA was performed on murine AH 4 weeks post-injection of virus. MMP-3 concentrations had increased by an average of 0.49 [0.11, 0.87] ng/ml in AAV-MMP-3 treated eyes (paired Student's *t*-test). (**E**) Aqueous MMP-3 activity was significantly increased by an average of 5.34 [1.12, 9.57] mU in AAV-MMP-3 treated eyes. Scale bars represent 50 μm. Asterisk symbol denotes a *P* value of < 0.05.

39–76% with an average of 59% (Fig. 6G). The differences between control and experimental eyes for each pair ranged from 16 to 26%, which corresponded to a statistically significant increase in the proportion of open space underlying the inner wall with AAV-MMP-3 relative to AAV-Null ($P = 0.002$, $n = 4$; paired Student's *t*-test). These data indicate that reduced ECM material in the TM and along the inner wall of SC is associated with AAV-MMP-3 treatment and may explain the enhanced outflow facility and IOP reduction. Furthermore, these morphological changes, because they were absent from controls, could not be attributed to an inflammatory or lytic response to AAV alone.

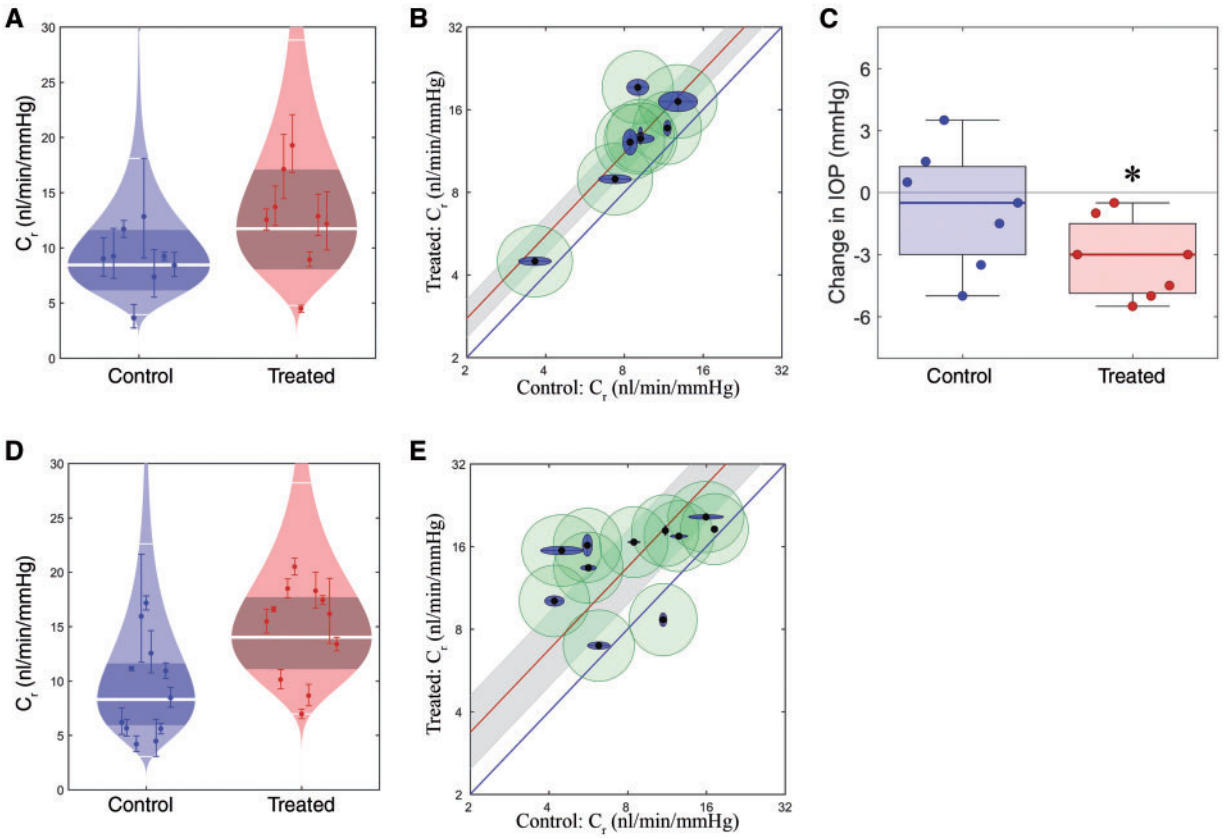

Figure 5. Effect of ECM remodelling on outflow facility and IOP. (**A**) 'Cello' plot depicting individual outflow facility values for eyes at 8 mmHg (Cr) and statistical distribution of both control (AAV-Null) and experimental (AAV-MMP-3) groups. Each point represents a single eye with 95% CI on C_r. Log normal distribution is shown, with the central white band showing the geometric mean and the thinner white bands showing two geometric standard deviations from the mean. The shaded region represents the 95% CI on the mean. (**B**) Paired outflow facility plot. Each inner point represents an eye pair, with log-transformed facilities of the control eye plotted on the x axis, and treated eye on the y axis. Outer blue and green ellipses show uncertainties generated from fitting the data to a model, intra-individual and cannulation variability respectively. Average increase is denoted by the red line, enclosed by a grey 95% CI, indicating significantly increased facility (does not overlap the blue unity line). (**C**) Box plots showing the change in IOP in treated and control eyes. Boxes show interquartile range and error bars represent the 5th and 95th percentiles. A significant reduction in IOP is observed in AAV-MMP-3 treated eyes (Wilcoxon signed-rank test). (**D-E**) Cello and paired facility plots for inducible AAV data sets.

Discussion

Matrix metalloproteinases are key regulators in the remodelling of extracellular matrices in the JCT region of the TM. Dysregulation of MMP expression and loss of MMP/TIMP homeostasis in glaucomatous AH have been associated with abnormal fibrillary ECM accumulation in the JCT region of POAG eyes (49–53). Furthermore, perfusion of anterior segments with purified MMPs increased outflow facility, while the use of metalloproteinase inhibitors (TIMP, minocycline) reduced outflow rates (30). Consistent with these findings, upregulation of MMPs following clinical laser treatment has been associated with the ocular hypotensive effect of trabeculoplasty (54,55). It is therefore apparent that the reduction in ECM turnover within the outflow tissues contributes to increased outflow resistance, and strategies specifically targeting outflow ECM may be effective in reducing outflow resistance. In this study, we focused on the development of a gene-based therapy for the delivery of MMP-3 into outflow tissues to facilitate aqueous outflow and reduce IOP.

It has been reported that the activity of a range of regulatory cytokines and growth factors found in AH directly impacts permeability in the outflow tissue, and many of these are known to be dysregulated in POAG AH (56,57). In particular, cytokines such as IL-1, TGF and TNF are known to influence the expression and secretion of ECM modulators, including MMPs in outflow tissues (58–60). It was therefore of interest to assess how POAG AH may affect the MMP-3 secretion and their relative activity in outflow cell culture systems.

We performed permeability assays with AH-treated SCEC and HTM monolayers to demonstrate that dysregulated MMP's in POAG AH influence monolayer permeability via modified ECM remodelling. (12,61). SCEC monolayers showed decreased permeability *in vitro* in response to glaucomatous AH, and this decrease was associated with a reduction in extracellular MMP-3 activity. HTM cells exhibited similar reductions in permeability. In contrast, treatment of cell monolayers exclusively with recombinant MMP-3 elevated monolayer permeability in comparison to controls, suggesting that MMP-3 could correct the permeability lowering effects of POAG aqueous. Because MMP-3 has previously been associated with apoptotic behaviour in Chinese hamster ovary cells and osteoclasts (62,63), we evaluated the effect of a wide concentration range of MMP-3 on SCEC and HTM viability. This way, we confirm that increases in paracellular permeability were not related to an MMP-3 cytotoxic effect, but rather its proteolytic activities, which these data support. More importantly, even lower concentrations of MMP-3 were detected *in vivo* in murine AH after AAV-mediated MMP-3 secretion (1.37 [0.89, 1.84] ng/ml, Fig. 4D) than those used in *in vitro* experiments. Collectively, these results indicate that a

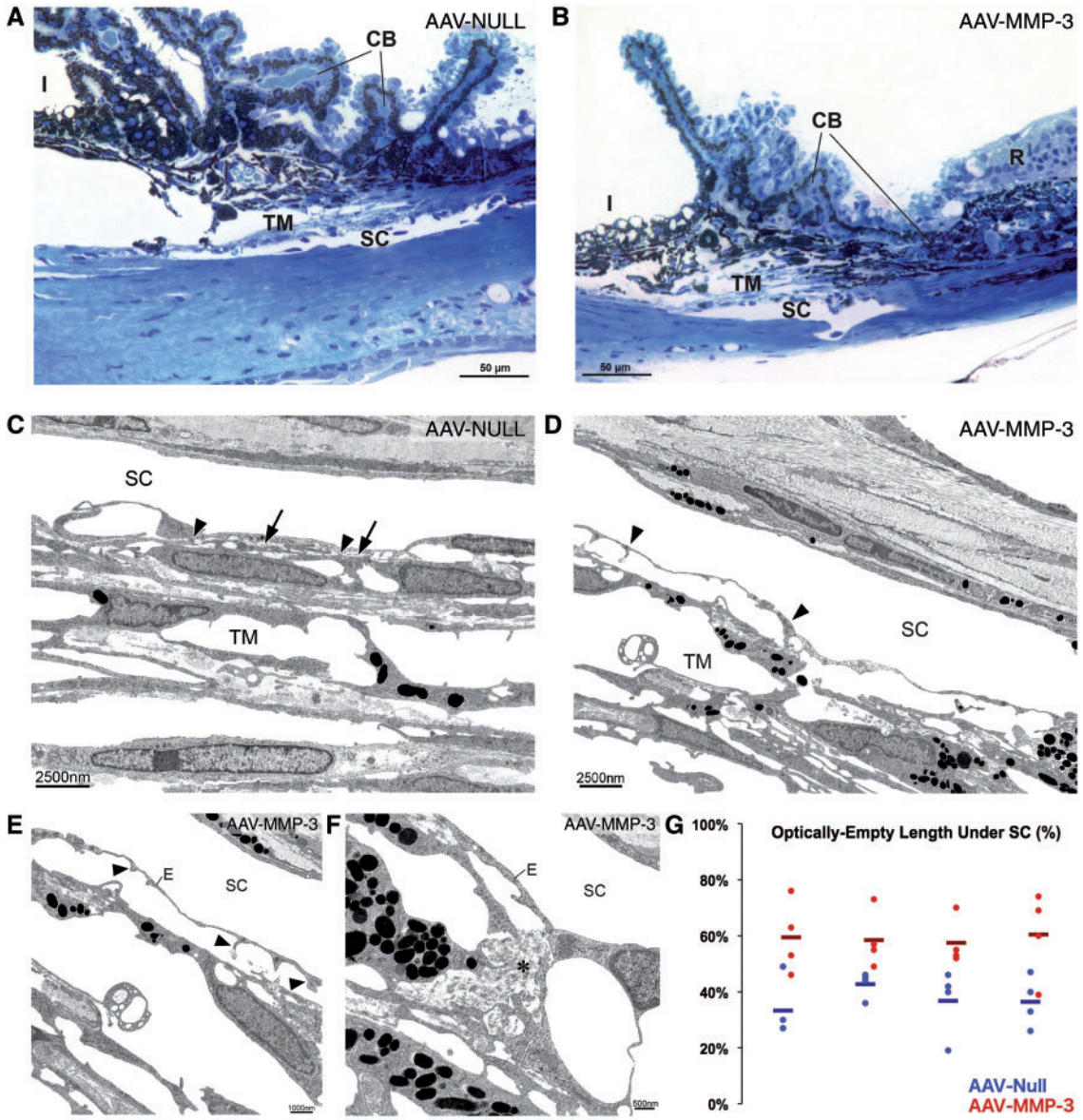

Figure 6. Transmission electron microscopy (TEM) analysis of ECM remodelling in outflow tissues. Semi-thin sections of the iridocorneal angle in mouse eyes treated with either (**A**) AAV-Null or (**B**) AAV-MMP-3. AAV-MMP-3 treated eyes show greater inter-trabecular spaces in outer trabecular meshwork (TM) than controls. Scale bar denotes 50 μm. (**C,D**) Transmission electron micrograph of the inner wall of Schlemm's Canal (SC) and the outer TM. (C) Control eye illustrating normal attachment between foot-like extensions of the inner wall endothelium and subendothelial cells (arrowheads), as well as with the discontinuous basement-membrane material underlying the inner wall endothelium (arrows). (D) Representative TEM image of an MMP-3 treated eye showing a disconnection of the inner wall endothelium from the subendothelial cells and the ECM (arrowheads). The widened subendothelial region lacks basement-membrane material and other ECM components. (**E,F**) Higher magnification of the inner wall of a treated eye. (E) Foot-like extensions of the inner wall endothelium (E) have disconnected from the subendothelial cells and the ECM (arrowheads), and the lack of ECM in this region is shown. (F) In other regions of treated eyes, clumps of presumably degraded ECM-material are localised underneath the inner wall of SC (asterisk). Such clumps of ECM are not present in controls. Scale bars are denoted on each image. CB = ciliary body, I = iris, R = retina. (**G**). Morphometric measurements of the optically empty space immediately underlying SC from four regions of contralateral eyes treated with AAV-MMP-3 (red data points) or AAV-Null (blue data points). Bars indicate average values for each eye. Contralateral eyes are presented immediately next to one another.

plausible target for MMP-3 activity is likely to be the ECM of TM and the inner wall endothelium of SC. This further contributes to the body of evidence demonstrating that the molecular pathological effects of glaucomatous AH are due, in part, to dysregulations of MMP-mediated remodelling and that induced elevations in MMP-3 expression in outflow tissues will have an enhancing effect on increasing aqueous outflow.

Previously, perfusion of explants of human anterior segments with a mixture of MMP-3, -2, -9 has been shown to result in an increase in outflow facility to 160% of baseline level (30). It has also been demonstrated that increases in IOP lead to an up-regulation of MMP-2, -3 and -14 through mechanical stretching of the TM and a reduction in TIMP2 (31,64–68). Such observations support the concept that controlled expression of MMPs within the anterior chamber holds therapeutic potential in regard to facilitating aqueous outflow. The inner wall endothelium of SC along with its basement membrane and JCT modulate the resistance to outflow. The interconnections between all components responsible for the outflow resistance generation is essential to maintain the homeostasis of outflow

drainage (11). Thus, targeting the ECM for remodelling in the JCT region using MMPs may effectively increase permeability of surrounding cells, thus increasing AH outflow rate and lowering IOP.

Owing to the fact that MMP-3 is a secretory enzyme, transduction of the corneal endothelium with AAV-MMP-3 will result in the secretion and delivery of the protein to the outflow tissues by following the natural flow of AH in the anterior chamber. *Ex vivo* studies in human corneas or corneal fibroblasts have demonstrated the potential and efficiency of delivering AAV to this tissue type (69,70). Successful transfection of different layers in the rabbit cornea by recombinant AAV further supports the potential of recombinant/exogenous protein delivery from corneal cells (71). Thus, it is likely that secreted MMP-3, expressed by corneal endothelia, will be directed toward the outflow tissue and activated with the aid of existing endogenous MMP-3 after which it will then be available for remodelling a range of ECM components. Attaining exclusive AAV expression in the cornea was obtained by using a single stranded AAV-2/9, as although single stranded AAV may enter other cells such as the TM, self-complementary viruses are required for sufficient DNA replication, and hence transduction of these cells (72).

The current data provide a direct proof of concept that AAV-mediated expression of MMP-3 from corneal endothelium decreases IOP with a concomitant increase in the rate of AH outflow through the drainage channels *ex vivo*. A number of parameters will require further refinement in order to address the translational feasibility of this approach. Although significant elevations in transient MMP-3 were found in murine AH post-treatment with AAV-MMP-3, these were well within tolerable limits as defined by our *in vitro* experiments (Fig. 2E and F). These MMP-3 elevations in AH (Fig. 4D), along with visually translucent corneas of normal thickness (Supplementary Material, Fig. S2), suggests that MMP-3 is preferentially secreted apically into the AH. MMP-3 expressed in the corneal endothelial cell layer is in the inactive form, which requires secretion for cleavage-induced activation, and is therefore unlikely to induce remodelling or damage to the endothelium itself. Activation is likely to occur in the AH after secretion, or extracellularly within the outflow tissues in the presence of other proteases. The observed elevation in aqueous MMP-3 activity indicates that activation at least begins in the AH (Fig. 4E). However, sustained expression of MMP-3, as would occur following permanent transfection of cells of the anterior chamber, could result in off-target proteolysis over time. A potentially more effective approach will be to employ an inducible promoter to drive MMP-3 expression on a periodic basis once the virus has been introduced into the anterior segment tissues of the eye. It is of note that the use of glucocorticoid-inducible promoters has been explored in this regard in adenoviral and AAV delivery systems to express MMP-1 in tissues of the TM (46). However, the use of a steroid response promoter may not be ideally suited from a therapeutic standpoint in humans, as activation of the promoter would require continuous exposure to steroid components, which can lead to abnormal IOP elevation (73–75). Glucocorticoids have also been shown to influence gene expression, which may play a pathogenic role in developing hypertension (76). Hence, we explored the effectiveness of a tetracycline-inducible system to express MMP-3 from the corneal endothelia, which allows for controllable and reversible activation by topically applied eye drops. We noted that activation of AAV for over 10 days was sufficient to significantly increase outflow facility *ex vivo* in mice and suggest that incorporation of other tetracycline derivatives may further enhance the effectiveness of the promoter and hence MMP-3 production. Our observed increase in facility of 68 [24, 128] % rivals that of conventional prostaglandin analogues which are in current use to treat glaucoma, noted to have an increase of 56 [−4, 154] % in the case of PDA205, also using the iPerfusion system (47).

To date, in studies utilising MMPs for increasing outflow or reducing IOP little emphasis has been given to the mechanism of action. Here, we show that MMP-3-mediated remodelling of specific ECM components is likely responsible for increased outflow, and hence, decreased IOP. Reductions in intensity and distribution of core ECM materials including collagen IV and laminin were observed *in vitro*, along with the disorganisation of the fibronectin meshwork and constrictions in the actin skeleton. These modifications suggest the development of a porous nature within the ECM of these monolayers. Semi-quantitation via western blot analysis coincides with these results, showing significant reductions in collagen IV, α-SMA and laminin proteins in the cell lysate fraction, where ECM proteins are likely to reside as no significant changes were displayed in media samples. It is reasonable to assume that these extracellular changes contribute to the observed alterations in electrical resistance and paracellular flux. Ultrastructural analysis of AAV-MMP-3 treated mouse eyes also showed reductions in ECM material at the sub-endothelial/JCT region, including areas of degraded ECM and widened inter-trabecular spaces. Upon quantification, these areas optically lacking ECM material were found to be consistently increased in response to MMP-3 both between regions of the anterior chamber and between treated eyes. Tight junctions remained intact after incubation with AAV-MMP-3 (Supplementary Material, Fig. S5), contrary to previous studies which have shown tight junction degradation by MMPs (77,78); validating that MMP-3 may primarily augment cell monolayer permeability via other mechanisms such as alteration of ECM components. These data indicate that a reduction in ECM material in the TM and inner wall of SC is responsible for the enhancement of outflow facility and consequently lowering of IOP in the treated eyes. The data also show that the reduction in ECM is not due to an inflammatory response that secondarily induces lytic enzymes in the treated eyes but most likely to the induction of MMP-3 through the treatment directly.

We show here for the first time that a topical eye drop regime can control the expression of a gene therapy vector utilised to reduce outflow resistance and IOP through ECM remodelling. The current approach may hold substantial potential as an effective human therapy should long-term safety and efficacy prove successful in non-human primates.

Materials and Methods

Cell culture

Human SCEC were isolated, cultured and fully characterised according to previous protocols (79–81). Briefly, cells were isolated from the SC lumen of human donor eyes using a cannulation technique. Isolated cells were tested for positive expression of VE-cadherin and fibulin-2, but absence of myocilin induction upon treatment with 100 nM dexamethasone for 5 days. Confluent cells displayed a characteristic linear fusiform morphology, were contact inhibited and generated a net transendothelial electrical resistance (TEER) greater than 10 $\Omega.cm^2$. TEER values were confirmed again prior to MMP-3 treatments. SCEC strains used were SC82 and SC83 between passages 2 and 7. Dulbecco's modified eagle medium (Gibco, Life Sciences) 1%

Pen/Strep/glutamine (Gibco, Life Sciences) and 10% foetal bovine serum (FBS) performance plus (Gibco, Life Sciences) was used as culture media in a 5% CO_2 incubator at 37 °C. Cells were passaged with trypsin-EDTA (Gibco-BRL) and seeded into 12 well or 24 well transwell plates (Costar, Corning). Human trabecular meshwork (HTM) cells were isolated and fully characterised according to the procedures described in (82–85). TM tissue is removed from human donor eyes using a blunt dissection technique, and TM cells are dissociated from the tissue using a collagenase digestion protocol as previously described (82). Isolated cells are characterised by their dramatic induction of myocilin protein following treatment with dexamethasone (100 nM) for 5 days as detailed before (79). HTM123 and HTM134 cells were cultured similar to SCEC's and matured for one week in 1% FBS media prior to treatment.

Human AH samples (detailed below) were added 1:10 to fresh media for cellular treatment for use with TEER and permeability assays as described below.

Recombinant human active MMP-3 (ab96555, Abcam) was added to cell media at a concentration of 10 ng/ml for TEER, permeability assays, western blotting and immunocytochemistry as described below. Inactivated MMP-3 controls were achieved by incubating active MMP-3 (10 ng/ml) with recombinant human active TIMP-1 (100 ng/ml, ab82104, Abcam) in cell media for 1 h prior to treatment.

Animals

Animals and procedures used in this study were carried out in accordance with regulations set out by The Health Products Regulatory Authority (HPRA), responsible for the correct implementation of EU directive 2010/63/EU. 8–11-week-old male and female C57BL/6 mice were used in all experimentation outlined in this study. Animals were bred and housed in specific-pathogen-free environments in the University of Dublin, Trinity College and all injections and IOP measurements complied with the HPRA project authorisation number AE19136/P017.

Patient aqueous humour samples

Human aqueous was obtained from the Mater Misericordiae Hospital, Dublin, Ireland. Upon informed consent, AH samples were collected from both POAG and control patients undergoing routine cataract surgery. The criteria for POAG was defined as the presence of glaucomatous optic disc cupping with associated visual field loss in an eye with a gonioscopically open anterior drainage channel, with an intraocular pressure $>$ 21 mmHg (86). The samples were taken immediately prior to corneal incision at the start of the procedure using a method described previously (87). Human AH collection conformed to the WMA Declaration of Helsinki and was approved by the Mater Misericordiae University Hospital Research Ethics Committee.

TEER measurement

Electrical resistance values were used as a representative of the integrity of the endothelial cell-cell junctions. Cells grown on Costar transwell-polyester membrane inserts with a pore size of 0.4 μm were treated with 10 ng/ml MMP-3 as described above. TEER readings were measured before and 24 h after treatment. An electrical probe (Millicell ERS-2 Voltohmmeter, Millipore) was placed into both the apical and basal chambers of the transwells and a current was passed through the monolayers, reported as a resistance in $\Omega.cm^2$. A correction was applied for the surface area of the membrane (0.33 cm^2) and for the electrical resistance of the membrane (blank transwell).

Permeability assessment by FITC-dextran flux

The extent of monolayer permeability was assessed by the basal to apical movement of a tracer molecule through the monolayer. Measures of permeability were taken 24h after treatment immediately after TEER values, keeping experimental set-up identical to that of TEER readings. The permeability protocol was repeated as described in (88). A 70 kDa fluorescein isothiocyanate (FITC)-conjugated dextran (Sigma) was added to the basal compartment of the transwell. Fresh medium was applied to the apical chamber and aliquots of 100 μl were taken every 15 min for a total of 120 min, replacing with fresh media. Sample aliquots were analysed for FITC fluorescence (FLUOstar OPTIMA, BMG Labtech) at an excitation wavelength of 492 nm and emission wavelength of 520 nm. Relative fluorescent units (RFU) were converted to their corresponding concentrations by interpolating from a known standard curve. Corrections were made for background fluorescence and the serial dilutions generated over the experiments time course. P_{app} values were calculated representing the apparent permeability coefficient for control (PBS) and treatment (10 ng/ml MMP-3). This was achieved via the following equation:

$$P_{app}(cm/s) = (dM/dT)/(A \times C_0),$$

Where dM/dT is the rate of appearance of FITC-dextran (FD) (μg/s) in the apical chamber from 0 to 120 min after the introduction of FD into the basal chamber. A is the effective surface area of the insert (cm^2) and C_0 is the initial concentration of FD in the basal chamber.

Cell viability

Cultured cells were treated with increasing concentrations of recombinant human MMP-3 (ab96555, Abcam) from 0 to 200 ng/ml. Cell viability was assessed 24 h post-treatment with MMP-3 using a CellTitre 96® AQueous One Solution Cell Proliferation Assay (Promega). Cell media was aspirated and a 1 in 6 dilution of the supplied reagent in media was added to the cell surface. Cells were incubated at 37 °C for 1 h and the media/reagent was transferred to a 96-well plate for reading by spectrophotometry (Multiskan FC, Thermo Scientific) at 450 nm. Standard *in vitro* viability calculations fail to consider sample size and the biological significance of the data. Hence, a modified approach was taken to determine at which concentration SCEC's show a reduced tolerability to MMP-3. This was defined at an average of 85% viability over three cell samples. This conservative value ensures that a cell population would remain viable and still be able to proliferate. Anything lower should be regarded as MMP-3 intolerability i.e. reduced cell proliferation or cell death. Control samples (0 ng/ml MMP-3) were normalised to 100% viability and a linear model fitted to the normalised data. The MMP-3 concentration at which cells had an average of 85% viability was interpolated from the lower 95% confidence bound from this linear model. This value represents the concentration of MMP-3 at which the average of three cell samples would have a 97.5% chance of retaining a greater to or equal than 85% viability.

Immunocytochemistry (cell monolayers)

Immunocytochemistry was performed to visualise changes in ECM composition in response to MMP-3. Human SCEC and HTM were grown on chamber slides (Lab-Tek II) and fixed in 4% paraformaldehyde (pH 7.4) for 20 min at room temperature and then washed with PBS for 15 min. Cell monolayers were blocked in PBS containing 5% normal goat serum (10658654, Fischer Scientific) and 0.1% Triton X-100 (T8787, Sigma) at room temperature for 30 min. Primary antibodies of collagen IV (ab6586, Abcam), α-SMA (ab5694, Abcam), laminin (ab11575, Abcam) and F-actin (A12379, ThermoFisher Scientific) were diluted at 1:100 in blocking buffer and incubated overnight at 4 °C. Secondary antibodies (ab6939, Abcam) were diluted at 1:500 in blocking buffer and then incubated for 2 h at room temperature. Following incubation, chamber slides were mounted with aqua-polymount (Polyscience) after nuclei-counterstaining with DAPI. Fluorescent images of SCEC monolayers were captured using a confocal microscope (Zeiss LSM 710), and processed using imaging software ZEN 2012.

For clear fibronectin (ab23750, Abcam) staining, cells were grown on cover slips and subsequently decellularised, leaving only the ECM material. Round cover slips (15 mm Diameter, Sparks Lab Supplies) were silanised before cell seeding to enhance binding to ECM products. This was achieved by initially immersing slips in 1% acid alcohol (1% concentrated HCL, 70% ethanol, 29% dH_2O) for 30 mins. Slips were washed in running water for 5 min, immersed in dH_2O twice for 5 min, immersed in 95% ethanol twice for 5 min and let air dry for 15 min. Cover slips were then immersed in 2% APES (3-aminopropyl triethoxysilane (A3648, Sigma) in acetone (Fisher Chemical)) for 1 min. Slips were again washed twice in dH_2O for 1 min and dried overnight at 37 °C. Cells were grown to confluency on these cover slips and, following treatment, were decellularised. This was achieved by consecutive washes in Hank's Balanced Salt Solution (HBSS), 20 mM ammonium hydroxide (Sigma) with 0.05% Triton X-100, and finally HBSS again. Matrices were fixed and stained as described above with chamber slides.

Western blotting

Cells were treated with 10 ng/ml MMP-3 for 24 h in serum-free media. Media supernatants were aspirated and mixed 1:6 with StrataClean resin (Agilent). After centrifugation, the supernatant was removed and the pellet was resuspended in NP-40 lysis buffer containing 50 mM Tris pH 7.5, 150 mM NaCL, 1% NP-40, 10% SDS, 1X protease inhibitor (Roche). Cells were lysed using NP-40 lysis buffer for protein collection. Samples were centrifuged at 10,000 rpm for 15 min (IEC Micromax microcentrifuge) and supernatant was retained. Protein samples were loaded onto a 10% SDS-PAGE gel at 30–50μg per well. Proteins were separated by electrophoresis over the course of 150 min at constant voltage (120 V) under reducing conditions and subsequently electro-transferred onto methanol-activated PVDF membranes at constant voltage (12 V). Gels intended for use with Collagen IV antibodies were run under native conditions. Membranes were blocked for 1 h at room temperature in 5% non-fat dry milk and incubated overnight at 4 °C with a rabbit primary antibodies to collagen IV, α-SMA, laminin and fibronectin as previously stated at concentrations of 1 in 1000 but 1 in 500 for laminin. Membrane blots were washed 3x5 min in TBS and incubated at room temperature for 2 h with horse radish peroxidase-conjugated anti-rabbit secondary antibody (Abcam). Blots were again washed and treated with a chemiluminescent substrate (WesternBright ECL, Advansta) and developed on a blot scanner (C-DiGit, LI-COR). The membranes containing cell lysate samples were re-probed with GAPDH antibody (ab9485, Abcam) for loading control normalisation. Media samples were normalised against their total protein concentration as determined by a spectrophotometer (ND-1000, NanoDrop). A total of four replicate blots were quantified for each cell lysate sample antibody, and 2–3 replicates for a media sample. Band images were quantified using Image J software. Fold change in band intensity was represented in comparison to vehicle control treatments of PBS.

AAV

AAV-2/9 containing the enhanced green fluorescent protein (eGFP) reporter gene (Vector Biolabs) was initially used to assess viral transduction and expression in the anterior chambers of wild type mice (C57/BL6). Murine MMP-3 cDNA was incorporated into Bam HI/Xhol sites of the pAAV-MCS vector (Cell Biolabs Inc) for constitutive expression of MMP-3. A null virus was used as contralateral control using the same capsid and vector. The inducible vector was designed by cloning MMP-3 cDNA into a pSingle-tTS (Clontech) vector. This vector was then digested with BsrBI and BsrGI and the fragment containing the inducible system and MMP-3 cDNA was ligated into the Not1 site of expression vector pAAV-MCS, to incorporate left and right AAV inverted terminal repeats (L-IRT and R-ITR). AAV-2/9 was generated using a triple transfection system in a stable HEK-293 cell line (Vector Biolabs). For animals injected with the inducible virus, after a 3-week incubation period, 0.2% doxycycline (D9891, Sigma) in PBS was administered twice daily to the eye for 10–16 days to induce viral expression. A similar inducible virus expressing eGFP was used as a control in the inducible study.

Intracameral injection

Animals were anaesthetised by intra-peritoneal injection of ketamine (Vetalar V, Zoetis) and domitor (SedaStart, Animalcare) (66.6 and 0.66 mg/kg, respectively). Pupils were dilated using one drop of tropicamide and phenylephrine (Bausch & Lomb) on each eye. 2 μl of virus at a stock titre of $5x10^{13}$ vector genomes per ml was initially back-filled into a glass needle (ID1.0 mm, WPI) attached via tubing (ID-1.02 mm, OD-1.98 mm, Smiths) to a syringe pump (PHD Ultra, Harvard Apparatus). An additional 1 μl of air was then withdrawn into the needle. Animals were injected intracamerally just above the limbus. Viral solution was infused at a rate of 1.5 μl/min for a total of 3 μl to include the air bubble. Contralateral eyes received an equal volume and titre of either AAV-MMP-3 or AAV-Null. The air bubble prevented the reflux of virus/aqueous back through the injection site when the needle was removed. Fucidic gel (Fucithalmic Vet, Dechra) was applied topically following injection as an antibiotic agent. To counter anaesthetic, Antisedan (atipamezole hydrochloride, SedaStop, Animalcare) was intra-peritoneally injected (8.33 mg/kg) and a carbomer based moisturising gel (Vidisic, Bausch & Lomb) was applied during recovery to prevent corneal dehydration.

Immunohistochemistry (mouse eyes)

Eyes were enucleated 4 weeks post-injection of virus and fixed in 4% paraformaldehyde overnight at 4 °C. The posterior

segment was removed by dissection and anterior segments were washed in PBS and placed in a sucrose gradient of incrementing sucrose concentrations containing 10%, 20% and finally 30% sucrose in PBS. Anterior segments were frozen in O.C.T compound (VWR Chemicals) in an isopropanol bath immersed in liquid nitrogen and cryosectioned (CM 1900, Leica Microsystems) at 12 μm thick sections. Sections were gathered onto charged Polysine® slides (Menzel-Gläser) and blocked for 1 h with 5% normal goat serum (10658654, Fischer Scientific) and 0.1% Triton X-100 in PBS. Slides were incubated overnight at 4 °C in a humidity chamber with a 1:100 dilution of primary antibody. Antibodies used were MMP-3 (ab52915, Abcam) and GFP (Cell Signalling). Sections were washed three times in PBS for 5 min and incubated with a Cy-3 conjugated anti-rabbit IgG antibody (ab6936, Abcam) at a 1:500 dilution for 2 h at 37 °C in a humidity chamber. Slides were washed as before and counter stained with DAPI for 30 s. Slides were mounted using Aquamount (Hs-106, National Diagnostics) with coverslips (Deckgläser) and visualised using a confocal microscope (Zeiss LSM 710).

Total MMP-3 quantification

MMP-3 concentration was quantified using enzyme-linked immunosorbent assay (ELISA) kits for both human SC monolayers (DMP300, R&D Systems) and murine aqueous (RAB0368-1KT, Sigma) according to the manufacturer's protocol. SC monolayers were cultured and treated with a 1 in 10 dilution of human cataract and POAG AH, a method previously described (87). Media was taken from the monolayers 24 h post-treatment and assayed for total MMP-3.

To measure the secretion of MMP-3 by AAV-2/9 into the AH, animals were inoculated with virus as described previously via intracameral injection. Four weeks post-injection, the animals were sacrificed and AH was collected. This was achieved by the cannulation of the cornea with a pulled glass needle (1B100-6, WPI) and gentle pressing of the eye until it was deflated. Aqueous was expelled from the needle (approximately 5 μl) by the attachment of a 25ml syringe connected via barb fitting and tubing (Smiths Medical) and a gradual push of the syringe plunger. Aqueous was assayed using the previously mentioned ELISA kit.

MMP-3 activity assay (FRET)

Enzymatic activity of secreted MMP-3 was quantified using fluorescence resonance energy transfer (FRET). A fluorescent peptide consisting of a donor/acceptor pair remains quenched in its intact state. This peptide contains binding sites specific to MMP-3. Once cleavage occurs through MMP-3 mediated proteolysis, fluorescence is recovered by the transfer of energy from the donor to the acceptor, resulting in an increase in the acceptor's emission intensity. Cleavage of substrate, and therefore fluorescence, was monitored on a FLUOstar OPTIMA (BMG Labtech) over the course of 2.5 h at 37 °C, to allow ample time for substrate cleavage. Media samples were collected from treated SC monolayers and combined with a 1:100 dilution of an MMP-3 specific substrate (ab112148, Abcam). Levels of active MMP-3 were interpolated from a standard curve defined by ELISA. For murine aqueous MMP-3 activity, aqueous was retrieved four weeks post-injection of AAV-MMP-3 or AAV-Null as described above. Aqueous samples were processed through an activity kit (abe3730, Source Bioscience), selected for its high sensitivity and specificity, according to the manufacturer's protocol.

Enzymatic activity was calculated as described in MMP-3 activity Assay Kit's (ab118972, Abcam) protocol:

$$\text{MMP}-3\ \text{Activity}\ (\text{nmol/min/ml}) = \frac{B\ \times\ \textit{Dilution Factor}}{(T2-T1)\ \times\ V},$$

Where B is the level of MMP-3 interpolated from the standard curve, T1 is the time (min) of the initial reading, T2 is the time (min) of the second reading and V is the sample volume (ml) added to the reaction well. The units 'nmol/min/ml' are equivalent to 'mU/ml'.

Measurement of outflow facility

Animals were sacrificed for outflow facility measurement 4 weeks after injection of virus. Eyes were enucleated for *ex vivo* perfusion using the *iPerfusion*™ system as described in (47). Contralateral eyes were perfused simultaneously using two independent but identical iPerfusion systems. Each system comprises an automated pressure reservoir, a thermal flow sensor (SLG64-0075, Sensiron) and a wet-wet differential pressure transducer (PX409, Omegadyne), in order to apply a desired pressure, measure flow rate out of the system and measure the intraocular pressure respectively. Enucleated eyes were secured to a pedestal using a small amount of cyanoacrylate glue in a PBS bath regulated at 35 °C. Perfusate was prepared (PBS including divalent cations and 5.5mM glucose) and filtered (0.2 μm, GVS Filter Technology) before use. Eyes were cannulated using a bevelled needle (NF33BV NanoFil™, World Precision Instruments) with the aid of a stereomicroscope and micromanipulator (World Precision Instruments). Eyes were perfused for 30 min at a pressure of ~8 mmHg in order to acclimatise to the environment. Incrementing pressure steps were applied from 4.5 to 21 mmHg, while recording flow rate and pressure. Flow (Q) and pressure (P) were averaged over 4 min of steady data, and a power law model of the form

$$Q = C_r\left(\frac{P}{P_r}\right)^{\beta} P$$

was fit to the data using weighted power law regression, yielding values of C_r, the reference facility at reference pressure $P_r = 8$ mmHg (corresponding to the physiological pressure drop across the outflow pathway), and β, a nonlinearity parameter characterising the pressure-dependent increase in facility observed in mouse eyes (47).

IOP

IOP measurements were performed by rebound tonometry (TonoLab, Icare) both prior to intracameral injection and 4 weeks post-injection. Readings, which were the average IOP values after five tonometric events, were taken 10 min after the intraperitoneal administration of mild general anaesthetic (53.28 mg/kg ketamine and 0.528 mg/kg domitor). Two readings were taken for one eye, then the other. This was repeated for a total of four readings per eye. Due to a minimum reading of 7 mmHg by the tonometer, a non-parametric approach was taken in the analysis of the readings. The median IOP was

calculated for each eye, and MAD (median absolute deviation) values were used as a measure of dispersion. For comparing median values in a paired population, the Wilcoxon matched-pairs signed-rank test was employed to test for changes in IOP pre- and post-injection, and also for changes between contralateral eyes.

Analysis of central corneal thickness

Enucleated mouse eyes transduced with AAV-MMP-3 or its contralateral control, AAV-Null, were fixed overnight in 4% PFA and washed in PBS. Posterior segments were removed by dissection under the microscope and anterior segments were embedded in medium (Tissue-Tek OCT Compound). Serial sectioning was performed on each eye and five frozen sections (12 μm) were transferred to a Polysine slide (Thermo Scientific) for staining with DAPI and mounted with aqua-polymount (Polyscience). Corneal sections were judged to be central by qualitatively taking the same distance from both iridocorneal angles. For quantitation, we measured the corneal thickness of sections on five consecutive slides by light and confocal microscopy (Zeiss LSM 710). A total of 25 measurements were taken from each eye to represent mean central corneal thickness (μm) using the NIH ImageJ software.

Transmission electron microscopy

Ultrastructural investigation was performed by transmission electron microscopy (TEM) in four pairs of mouse eyes. One eye of each pair was injected with AAV-Null, the other with AAV-MMP-3, as described above. Four weeks after injection, the eyes were enucleated and immersion fixed in Karnovsky's fixative (2.5% PFA, 0.1M cacodylate, 2.25% glutaraldehyde and dH_2O) for 1 h. Eyes were then removed from fixative and the cornea pierced using a 30-gauge needle (BD Microlance 3, Becton Dickinson). Eyes were placed back into fixative overnight at 4 °C, washed 3x10 min, stored in 0.1M cacodylate and sent to Erlangen.

Here the eyes were cut meridionally through the centre of the pupil, the lens carefully removed, and the two halves of each eye embedded in Epon. Semi-thin sagittal and then ultrathin sections of Schlemm's canal (SC) and trabecular meshwork (TM) were cut from one end of each half, and then the other approximately 0.2–0.3 mm deeper. The location of the superficial and deeper cut ends was alternated for the second half of the eye such that all four regions examined were at least 0.2–0.3 mm distant from one another. The ultrathin sections contained the entire anterior posterior length of the inner wall and the TM.

In four regions of each eye, we measured the length of optically empty space immediately underlying the inner wall endothelium of SC (Supplementary Material, Fig. S6). We also measured the inner wall length in contact with ECM, including basement membrane material, elastic fibres, or amorphous material. The optically empty length divided by the total length (optically empty + ECM lengths) was calculated and defined as the percentage of optically empty length for that region. All measurements were performed at 10,000x magnification, with each region including approximately 100 individual lengths of ECM or optically empty space. The measurements were performed by the two authors: ELD and CFK.

Statistical analysis

For TEER values, activity units (mU/ml) and concentrations (ng/ml), statistical differences were analysed by using unpaired two-tailed Student's *t*-tests. Differences in P_{app} values (cm/s) were determined by a one way ANOVA with Tukey's correction for multiple comparisons, where appropriate. ELISA standard curve concentrations were log-transformed and absorbance values were fitted to a sigmoidal dose response curve with variable slope for interpolation. Fold change of western blot data was log-transformed and investigated for significance using a one-sample *t*-test against a theoretical mean of 0. To measure MMP-3 concentration and activity in the AH of wild type (WT) mice, a paired two-tailed *t*-test was carried out for contralateral samples. Outflow facility was analysed using a weighted paired *t*-test performed in MATLAB as described in (47), incorporating both system and biological uncertainties. For IOP data, median values were obtained to reflect the non-parametric nature of the tonometer, and the Wilcoxon matched-pairs signed rank test was used to compare changes in paired populations. For morphology, the distribution of values representing the percent optically empty length was first examined using a Shapiro-Wilk and Anderson-Darling tests to detect for deviations from a normal distribution. The percent optically empty length between contralateral eyes was then analysed using a paired Student's *t*-test. Statistical significance was inferred when $P < 0.05$ in all experimentation. Results were depicted as 'mean, [95% Confidence Intervals]' unless otherwise stated in the results section.

Supplementary Material

Supplementary Material is available at *HMG* online.

Acknowledgements

We wish to acknowledge Caroline Woods and Charles Murray for animal husbandry. We would also like to thank Elke Kretzschmar, Britta Bäckermann and Andrea Eichnorn for preparing the semi-and ultrathin sections and Marco Gößwein for his assistance in finalizing the TEM images for publication.

Conflict of Interest statement. None declared.

Funding

Research at the Ocular Genetics Unit at the University of Dublin, Trinity College was supported by the European Research Council [ERC-2012-AdG 322656-Oculus]. We also acknowledge an equipment grant from Science Foundation Ireland in support of this project [12/ERC/B2539]. Research at Imperial College London was supported by the US National Institutes of Health (EY022359 and EY019696), the UK Engineering and Physical Sciences Research Council (EP/J010499/1), and Fight for Sight UK (Ref 1385). Work at Duke University was also supported by the US National Institutes of Health (EY022359). Funding to pay the Open Access publication charges for this article was provided by the European Research Council.

References

1. Yan, X., Li, M., Chen, Z., Zhu, Y., Song, Y. and Zhang, H. (2016) Schlemm's Canal and Trabecular Meshwork in Eyes with Primary Open Angle Glaucoma: A Comparative Study Using High-Frequency Ultrasound Biomicroscopy. *PLoS One*, **11**, e0145824.

2. Lanza, M., Iaccarino, S., Mele, L., Carnevale, U.A., Irregolare, C., Lanza, A., Femiano, F. and Bifani, M. (2016) Intraocular pressure evaluation in healthy eyes and diseased ones using contact and non contact devices. *Cont. Lens. Anterior. Eye*, **39**, 154–159.
3. Grant, W.M. (1951) Clinical measurements of aqueous outflow. *Am. J. Ophthalmol.*, **34**, 1603–1605.
4. Rylander, N.R. and Vold, S.D. (2008) Cost analysis of glaucoma medications. *Am. J. Ophthalmol.*, **145**, 106–113.
5. Hamanaka, T. and Bill, A. (1988) Effects of alpha-chymotrypsin on the outflow routes for aqueous humor. *Exp. Eye Res.*, **46**, 323–341.
6. Johnson, M. (2006) 'What controls aqueous humour outflow resistance?' *Exp. Eye Res.*, **82**, 545–557.
7. Tanihara, H., Inatani, M., Koga, T., Yano, T. and Kimura, A. (2002) Proteoglycans in the eye. *Cornea*, **21**, 62–69.
8. Floyd, B.B., Cleveland, P.H. and Worthen, D.M. (1985) Fibronectin in human trabecular drainage channels. *Invest. Ophthalmol. Vis. Sci.*, **26**, 797–804.
9. Keller, K.E., Bradley, J.M., Vranka, J.A. and Acott, T.S. (2011) Segmental versican expression in the trabecular meshwork and involvement in outflow facility. *Invest. Ophthalmol. Vis. Sci.*, **52**, 5049–5057.
10. Swaminathan, S.S., Oh, D.J., Kang, M.H., Ren, R., Jin, R., Gong, H. and Rhee, D.J. (2013) Secreted protein acidic and rich in cysteine (SPARC)-null mice exhibit more uniform outflow. *Invest. Ophthalmol. Vis. Sci.*, **54**, 2035–2047.
11. Overby, D.R., Stamer, W.D. and Johnson, M. (2009) The changing paradigm of outflow resistance generation: towards synergistic models of the JCT and inner wall endothelium. *Exp. Eye Res.*, **88**, 656–670.
12. Curtis, T.M., McKeown-Longo, P.J., Vincent, P.A., Homan, S.M., Wheatley, E.M. and Saba, T.M. (1995) Fibronectin attenuates increased endothelial monolayer permeability after RGD peptide, anti-alpha 5 beta 1, or TNF-alpha exposure. *Am. J. Physiol.*, **269**, 248–260.
13. Stickel, S.K. and Wang, Y.L. (1988) Synthetic peptide GRGDS induces dissociation of alpha-actinin and vinculin from the sites of focal contacts. *J. Cell Biol.*, **107**, 1231–1239.
14. Lampugnani, M.G., Resnati, M., Dejana, E. and Marchisio, P.C. (1991) The role of integrins in the maintenance of endothelial monolayer integrity. *J. Cell Biol.*, **112**, 479–490.
15. Wu, M.H., Ustinova, E. and Granger, H.J. (2001) Integrin binding to fibronectin and vitronectin maintains the barrier function of isolated porcine coronary venules. *J. Physiol.*, **532**, 785–791.
16. Mehta, D. and Malik, A.B. (2006) Signaling mechanisms regulating endothelial permeability. *Physiol. Rev.*, **86**, 279–367.
17. Keller, K.E. and Acott, T.S. (2013) The Juxtacanalicular Region of Ocular Trabecular Meshwork: A Tissue with a Unique Extracellular Matrix and Specialized Function. *J. Ocul. Biol. Dis. Infor.*, **1**, 3.
18. Rohen, J.W., Futa, R. and Lutjen-Drecoll, E. (1981) The fine structure of the cribriform meshwork in normal and glaucomatous eyes as seen in tangential sections. *Invest. Ophthalmol. Vis. Sci.*, **21**, 574–585.
19. Faralli, J.A., Schwinn, M.K., Gonzalez, J.M., Jr., Filla, M.S. and Peters, D.M. (2009) Functional properties of fibronectin in the trabecular meshwork. *Exp. Eye Res.*, **88**, 689–693.
20. Tamm, E.R., Siegner, A., Baur, A. and Lutjen-Drecoll, E. (1996) Transforming growth factor-beta 1 induces alpha-smooth muscle-actin expression in cultured human and monkey trabecular meshwork. *Exp. Eye Res.*, **62**, 389–397.
21. Schlunck, G., Han, H., Wecker, T., Kampik, D., Meyer-ter-Vehn, T. and Grehn, F. (2008) Substrate rigidity modulates cell matrix interactions and protein expression in human trabecular meshwork cells. *Invest. Ophthalmol. Vis. Sci.*, **49**, 262–269.
22. Acott, T.S., Kelley, M.J., Keller, K.E., Vranka, J.A., Abu-Hassan, D.W., Li, X., Aga, M. and Bradley, J.M. (2014) Intraocular pressure homeostasis: maintaining balance in a high-pressure environment. *J. Ocul. Pharmacol. Ther.*, **30**, 94–101.
23. Nagase, H., Suzuki, K., Enghild, J.J. and Salvesen, G. (1991) Stepwise activation mechanisms of the precursors of matrix metalloproteinases 1 (tissue collagenase) and 3 (stromelysin). *Biomed. Biochim. Acta*, **50**, 749–754.
24. Schlotzer-Schrehardt, U., Lommatzsch, J., Kuchle, M., Konstas, A.G. and Naumann, G.O. (2003) Matrix metalloproteinases and their inhibitors in aqueous humor of patients with pseudoexfoliation syndrome/glaucoma and primary open-angle glaucoma. *Invest. Ophthalmol. Vis. Sci.*, **44**, 1117–1125.
25. Ronkko, S., Rekonen, P., Kaarniranta, K., Puustjarvi, T., Terasvirta, M. and Uusitalo, H. (2007) Matrix metalloproteinases and their inhibitors in the chamber angle of normal eyes and patients with primary open-angle glaucoma and exfoliation glaucoma. *Graefes Arch. Clin. Exp. Ophthalmol.*, **245**, 697–704.
26. Tektas, O.Y. and Lutjen-Drecoll, E. (2009) Structural changes of the trabecular meshwork in different kinds of glaucoma. *Exp. Eye Res.*, **88**, 769–775.
27. Overby, D.R., Bertrand, J., Tektas, O.Y., Boussommier-Calleja, A., Schicht, M., Ethier, C.R., Woodward, D.F., Stamer, W.D. and Lutjen-Drecoll, E. (2014) Ultrastructural changes associated with dexamethasone-induced ocular hypertension in mice. *Invest. Ophthalmol. Vis. Sci.*, **55**, 4922–4933.
28. Pang, I.H., Fleenor, D.L., Hellberg, P.E., Stropki, K., McCartney, M.D. and Clark, A.F. (2003) Aqueous outflow-enhancing effect of tert-butylhydroquinone: involvement of AP-1 activation and MMP-3 expression. *Invest. Ophthalmol. Vis. Sci.*, **44**, 3502–3510.
29. Webb, J.G., Husain, S., Yates, P.W. and Crosson, C.E. (2006) Kinin modulation of conventional outflow facility in the bovine eye. *J. Ocul. Pharmacol. Ther.*, **22**, 310–316.
30. Bradley, J.M., Vranka, J., Colvis, C.M., Conger, D.M., Alexander, J.P., Fisk, A.S., Samples, J.R. and Acott, T.S. (1998) Effect of matrix metalloproteinases activity on outflow in perfused human organ culture. *Invest. Ophthalmol. Vis. Sci.*, **39**, 2649–2658.
31. De Groef, L., Van Hove, I., Dekeyster, E., Stalmans, I. and Moons, L. (2013) MMPs in the trabecular meshwork: promising targets for future glaucoma therapies?. *Invest. Ophthalmol. Vis. Sci.*, **54**, 7756–7763.
32. Rehnberg, M., Ammitzboll, T. and Tengroth, B. (1987) Collagen distribution in the lamina cribrosa and the trabecular meshwork of the human eye. *Br. J. Ophthalmol.*, **71**, 886–892.
33. Medina-Ortiz, W.E., Belmares, R., Neubauer, S., Wordinger, R.J. and Clark, A.F. (2013) Cellular fibronectin expression in human trabecular meshwork and induction by transforming growth factor-beta2. *Invest. Ophthalmol. Vis. Sci.*, **54**, 6779–6788.
34. Hann, C.R., Springett, M.J., Wang, X. and Johnson, D.H. (2001) Ultrastructural localization of collagen IV, fibronectin, and laminin in the trabecular meshwork of normal and glaucomatous eyes. *Ophthalmic Res.*, **33**, 314–324.

35. Umihira, J., Nagata, S., Nohara, M., Hanai, T., Usuda, N. and Segawa, K. (1994) Localization of elastin in the normal and glaucomatous human trabecular meshwork. *Invest. Ophthalmol. Vis. Sci.*, **35**, 486–494.
36. Wirtz, M.K., Bradley, J.M., Xu, H., Domreis, J., Nobis, C.A., Truesdale, A.T., Samples, J.R., Van Buskirk, E.M. and Acott, T.S. (1997) Proteoglycan expression by human trabecular meshworks. *Curr. Eye Res.*, **16**, 412–421.
37. Murphy, G., Cockett, M.I., Stephens, P.E., Smith, B.J. and Docherty, A.J. (1987) Stromelysin is an activator of procollagenase. A study with natural and recombinant enzymes. *Biochem. J.*, **248**, 265–268.
38. Lijnen, H.R., Silence, J., Van Hoef, B. and Collen, D. (1998) Stromelysin-1 (MMP-3)-independent gelatinase expression and activation in mice. *Blood*, **91**, 2045–2053.
39. Ogata, Y., Enghild, J.J. and Nagase, H. (1992) Matrix metalloproteinase 3 (stromelysin) activates the precursor for the human matrix metalloproteinase 9. *J. Biol. Chem.*, **267**, 3581–3584.
40. Yang, Y., Estrada, E.Y., Thompson, J.F., Liu, W. and Rosenberg, G.A. (2007) Matrix metalloproteinase-mediated disruption of tight junction proteins in cerebral vessels is reversed by synthetic matrix metalloproteinase inhibitor in focal ischemia in rat. *J. Cereb. Blood Flow Metab.*, **27**, 697–709.
41. Yamada, H., Yoneda, M., Inaguma, S., Watanabe, D., Banno, S., Yoshikawa, K., Mizutani, K., Iwaki, M. and Zako, M. (2013) Infliximab counteracts tumor necrosis factor-alpha-enhanced induction of matrix metalloproteinases that degrade claudin and occludin in non-pigmented ciliary epithelium. *Biochem. Pharmacol.*, **85**, 1770–1782.
42. Rajashekhar, G., Shivanna, M., Kompella, U.B., Wang, Y. and Srinivas, S.P. (2014) Role of MMP-9 in the breakdown of barrier integrity of the corneal endothelium in response to TNF-alpha. *Exp. Eye Res.*, **122**, 77–85.
43. Buie, L.K., Rasmussen, C.A., Porterfield, E.C., Ramgolam, V.S., Choi, V.W., Markovic-Plese, S., Samulski, R.J., Kaufman, P.L. and Borras, T. (2010) Self-complementary AAV virus (scAAV) safe and long-term gene transfer in the trabecular meshwork of living rats and monkeys. *Invest. Ophthalmol. Vis. Sci.*, **51**, 236–248.
44. Bogner, B., Boye, S.L., Min, S.H., Peterson, J.J., Ruan, Q., Zhang, Z., Reitsamer, H.A., Hauswirth, W.W. and Boye, S.E. (2015) Capsid Mutated Adeno-Associated Virus Delivered to the Anterior Chamber Results in Efficient Transduction of Trabecular Meshwork in Mouse and Rat. *PLoS One*, **10**, e0128759.
45. Gerometta, R., Spiga, M.G., Borras, T. and Candia, O.A. (2010) Treatment of sheep steroid-induced ocular hypertension with a glucocorticoid-inducible MMP1 gene therapy virus. *Invest. Ophthalmol. Vis. Sci.*, **51**, 3042–3048.
46. Borras, T., Buie, L.K. and Spiga, M.G. (2016) Inducible scAAV2.GRE.MMP1 lowers IOP long-term in a large animal model for steroid-induced glaucoma gene therapy. *Gene Ther.*, **23**, 438–449.
47. Sherwood, J.M., Reina-Torres, E., Bertrand, J.A., Rowe, B. and Overby, D.R. (2016) Measurement of Outflow Facility Using iPerfusion. *PLoS One*, **11**, e0150694.
48. Overby, D.R., Bertrand, J., Schicht, M., Paulsen, F., Stamer, W.D. and Lutjen-Drecoll, E. (2014) The structure of the trabecular meshwork, its connections to the ciliary muscle, and the effect of pilocarpine on outflow facility in mice. *Invest. Ophthalmol. Vis. Sci.*, **55**, 3727–3736.
49. Nga, A.D., Yap, S.L., Samsudin, A., Abdul-Rahman, P.S., Hashim, O.H. and Mimiwati, Z. (2014) Matrix metalloproteinases and tissue inhibitors of metalloproteinases in the aqueous humour of patients with primary angle closure glaucoma - a quantitative study. *BMC Ophthalmol.*, **14**, 33.
50. Ashworth Briggs, E.L., Toh, T., Eri, R., Hewitt, A.W. and Cook, A.L. (2015) TIMP1, TIMP2, and TIMP4 are increased in aqueous humor from primary open angle glaucoma patients. *Mol. Vis.*, **21**, 1162–1172.
51. Badier-Commander, C., Verbeuren, T., Lebard, C., Michel, J.B. and Jacob, M.P. (2000) Increased TIMP/MMP ratio in varicose veins: a possible explanation for extracellular matrix accumulation. *J. Pathol.*, **192**, 105–112.
52. Lutjen-Drecoll, E., Shimizu, T., Rohrbach, M. and Rohen, J.W. (1986) Quantitative analysis of 'plaque material' between ciliary muscle tips in normal- and glaucomatous eyes. *Exp. Eye Res.*, **42**, 457–465.
53. Rohen, J.W., Lutjen-Drecoll, E., Flugel, C., Meyer, M. and Grierson, I. (1993) Ultrastructure of the trabecular meshwork in untreated cases of primary open-angle glaucoma (POAG). *Exp. Eye Res.*, **56**, 683–692.
54. Parshley, D.E., Bradley, J.M., Samples, J.R., Van Buskirk, E.M. and Acott, T.S. (1995) Early changes in matrix metalloproteinases and inhibitors after in vitro laser treatment to the trabecular meshwork. *Curr. Eye Res.*, **14**, 537–544.
55. Parshley, D.E., Bradley, J.M., Fisk, A., Hadaegh, A., Samples, J.R., Van Buskirk, E.M. and Acott, T.S. (1996) Laser trabeculoplasty induces stromelysin expression by trabecular juxtacanalicular cells. *Invest. Ophthalmol. Vis. Sci.*, **37**, 795–804.
56. Takai, Y., Tanito, M. and Ohira, A. (2012) Multiplex cytokine analysis of aqueous humor in eyes with primary open-angle glaucoma, exfoliation glaucoma, and cataract. *Invest. Ophthalmol. Vis. Sci.*, **53**, 241–247.
57. Chua, J., Vania, M., Cheung, C.M., Ang, M., Chee, S.P., Yang, H., Li, J. and Wong, T.T. (2012) Expression profile of inflammatory cytokines in aqueous from glaucomatous eyes. *Mol. Vis.*, **18**, 431–438.
58. Kelley, M.J., Rose, A.Y., Song, K., Chen, Y., Bradley, J.M., Rookhuizen, D. and Acott, T.S. (2007) Synergism of TNF and IL-1 in the induction of matrix metalloproteinase-3 in trabecular meshwork. *Invest. Ophthalmol. Vis. Sci.*, **48**, 2634–2643.
59. Bradley, J.M., Anderssohn, A.M., Colvis, C.M., Parshley, D.E., Zhu, X.H., Ruddat, M.S., Samples, J.R. and Acott, T.S. (2000) Mediation of laser trabeculoplasty-induced matrix metalloproteinase expression by IL-1beta and TNFalpha. *Invest. Ophthalmol. Vis. Sci.*, **41**, 422–430.
60. Alexander, J.P., Samples, J.R. and Acott, T.S. (1998) Growth factor and cytokine modulation of trabecular meshwork matrix metalloproteinase and TIMP expression. *Curr. Eye Res.*, **17**, 276–285.
61. Partridge, C.A., Jeffrey, J.J. and Malik, A.B. (1993) A 96-kDa gelatinase induced by TNF-alpha contributes to increased microvascular endothelial permeability. *Am. J. Physiol.*, **265**, 438–447.
62. Si-Tayeb, K., Monvoisin, A., Mazzocco, C., Lepreux, S., Decossas, M., Cubel, G., Taras, D., Blanc, J.F., Robinson, D.R. and Rosenbaum, J. (2006) Matrix metalloproteinase 3 is present in the cell nucleus and is involved in apoptosis. *Am. J. Pathol.*, **169**, 1390–1401.
63. Garcia, A.J., Tom, C., Guemes, M., Polanco, G., Mayorga, M.E., Wend, K., Miranda-Carboni, G.A. and Krum, S.A. (2013) ERalpha signaling regulates MMP3 expression to induce FasL cleavage and osteoclast apoptosis. *J. Bone Miner. Res.*, **28**, 283–290.

64. Bradley, J.M., Kelley, M.J., Rose, A. and Acott, T.S. (2003) Signaling pathways used in trabecular matrix metalloproteinase response to mechanical stretch. *Invest. Ophthalmol. Vis. Sci.*, **44**, 5174–5181.
65. Bradley, J.M., Kelley, M.J., Zhu, X., Anderssohn, A.M., Alexander, J.P. and Acott, T.S. (2001) Effects of mechanical stretching on trabecular matrix metalloproteinases. *Invest. Ophthalmol. Vis. Sci.*, **42**, 1505–1513.
66. Gonzalez, P., Epstein, D.L. and Borras, T. (2000) Genes upregulated in the human trabecular meshwork in response to elevated intraocular pressure. *Invest. Ophthalmol. Vis. Sci.*, **41**, 352–361.
67. Luna, C., Li, G., Liton, P.B., Epstein, D.L. and Gonzalez, P. (2009) Alterations in gene expression induced by cyclic mechanical stress in trabecular meshwork cells. *Mol. Vis.*, **15**, 534–544.
68. Vittitow, J. and Borras, T. (2004) Genes expressed in the human trabecular meshwork during pressure-induced homeostatic response. *J. Cell. Physiol.*, **201**, 126–137.
69. Lai, L., Lin, K., Foulks, G., Ma, L., Xiao, X. and Chen, K. (2005) Highly efficient ex vivo gene delivery into human corneal endothelial cells by recombinant adeno-associated virus. *Curr. Eye Res.*, **30**, 213–219.
70. Sharma, A., Ghosh, A., Hansen, E.T., Newman, J.M. and Mohan, R.R. (2010) Transduction efficiency of AAV 2/6, 2/8 and 2/9 vectors for delivering genes in human corneal fibroblasts. *Brain Res. Bull.*, **81**, 273–278.
71. Liu, J., Saghizadeh, M., Tuli, S.S., Kramerov, A.A., Lewin, A.S., Bloom, D.C., Hauswirth, W.W., Castro, M.G., Schultz, G.S. and Ljubimov, A.V. (2008) Different tropism of adenoviruses and adeno-associated viruses to corneal cells: implications for corneal gene therapy. *Mol. Vis.*, **14**, 2087–2096.
72. Borras, T., Xue, W., Choi, V.W., Bartlett, J.S., Li, G., Samulski, R.J. and Chisolm, S.S. (2006) Mechanisms of AAV transduction in glaucoma-associated human trabecular meshwork cells. *J. Gene Med.*, **8**, 589–602.
73. Herschler, J. (1976) Increased intraocular pressure induced by repository corticosteroids. *Am. J. Ophthalmol.*, **82**, 90–93.
74. Mandapati, J.S. and Metta, A.K. (2011) Intraocular pressure variation in patients on long-term corticosteroids. *Indian Dermatol. Online J.*, **2**, 67–69.
75. Pleyer, U., Ursell, P.G. and Rama, P. (2013) Intraocular pressure effects of common topical steroids for post-cataract inflammation: are they all the same? *Opthalmol. Ther.*, **2**, 55–72.
76. Clark, A.F., Steely, H.T., Dickerson, J.E., Jr., English-Wright, S., Stropki, K., McCartney, M.D., Jacobson, N., Shepard, A.R., Clark, J.I., Matsushima, H., *et al.* (2001) Glucocorticoid induction of the glaucoma gene MYOC in human and monkey trabecular meshwork cells and tissues. *Invest. Ophthalmol. Vis. Sci.*, **42**, 1769–1780.
77. Gurney, K.J., Estrada, E.Y. and Rosenberg, G.A. (2006) Blood-brain barrier disruption by stromelysin-1 facilitates neutrophil infiltration in neuroinflammation. *Neurobiol. Dis.*, **23**, 87–96.
78. Vermeer, P.D., Denker, J., Estin, M., Moninger, T.O., Keshavjee, S., Karp, P., Kline, J.N. and Zabner, J. (2009) MMP9 modulates tight junction integrity and cell viability in human airway epithelia. *Am. J. Physiol. Lung Cell Mol. Physiol.*, **296**, 751–762.
79. Stamer, W.D., Roberts, B.C., Howell, D.N. and Epstein, D.L. (1998) Isolation, culture, and characterization of endothelial cells from Schlemm's canal. *Invest. Ophthalmol. Vis. Sci.*, **39**, 1804–1812.
80. Perkumas, K.M. and Stamer, W.D. (2012) Protein markers and differentiation in culture for Schlemm's canal endothelial cells. *Exp. Eye Res.*, **96**, 82–87.
81. Heimark, R.L., Kaochar, S. and Stamer, W.D. (2002) Human Schlemm's canal cells express the endothelial adherens proteins, VE-cadherin and PECAM-1. *Curr. Eye Res.*, **25**, 299–308.
82. Stamer, W.D., Seftor, R.E., Williams, S.K., Samaha, H.A. and Snyder, R.W. (1995) Isolation and culture of human trabecular meshwork cells by extracellular matrix digestion. *Curr. Eye Res.*, **14**, 611–617.
83. Stamer, W.D., Seftor, R.E., Snyder, R.W. and Regan, J.W. (1995) Cultured human trabecular meshwork cells express aquaporin-1 water channels. *Curr. Eye Res.*, **14**, 1095–1100.
84. Stamer, W.D., Huang, Y., Seftor, R.E., Svensson, S.S., Snyder, R.W. and Regan, J.W. (1996) Cultured human trabecular meshwork cells express functional alpha 2A adrenergic receptors. *Invest. Ophthalmol. Vis. Sci.*, **37**, 2426–2433.
85. Stamer, W.D. and Clark, A.F. (2016) The many faces of the trabecular meshwork cell. *Exp. Eye Res*, in press.
86. Siah, W.F., Loughman, J. and O'Brien, C. (2015) Lower Macular Pigment Optical Density in Foveal-Involved Glaucoma. *Ophthalmology*, **122**, 2029–2037.
87. Wallace, D.M., Clark, A.F., Lipson, K.E., Andrews, D., Crean, J.K. and O'Brien, C.J. (2013) Anti-connective tissue growth factor antibody treatment reduces extracellular matrix production in trabecular meshwork and lamina cribrosa cells. *Invest. Ophthalmol. Vis. Sci.*, **54**, 7836–7848.
88. Keaney, J., Walsh, D.M., O'Malley, T., Hudson, N., Crosbie, D.E., Loftus, T., Sheehan, F., McDaid, J., Humphries, M.M., Callanan, J.J., *et al.* (2015) Autoregulated paracellular clearance of amyloid-beta across the blood-brain barrier. *Sci. Adv.*, **1**, e1500472.